High-order accurate discontinuous Galerkin simulation tool for fire modeling

Mark Lohry
Princeton University

8th International Aircraft Fire and Cabin Safety Research Conference
October 2016
Atlantic City, New Jersey

Outline

Motivation

- FAA requirement for alarms to go off within 60 seconds of fire ignition.
- Several different detection methods are generally used together, e.g. temperature, smoke/particulate, radiation, optical
- Their effectiveness is determined by the dynamics of a particular fire and their relative position.
- Accurate prediction of fire-induced flow in a cargo hold is a necessary first step to predicting detection capabilities.
- More reliable detection capabilities could potentially reduce false alarms.

B707 cargo geometry

- Experimental and computational data for B707 cargo fires available from work at Sandia and FAA Tech center.
- Current goal is to perform a direct comparison of those results with our new solver.

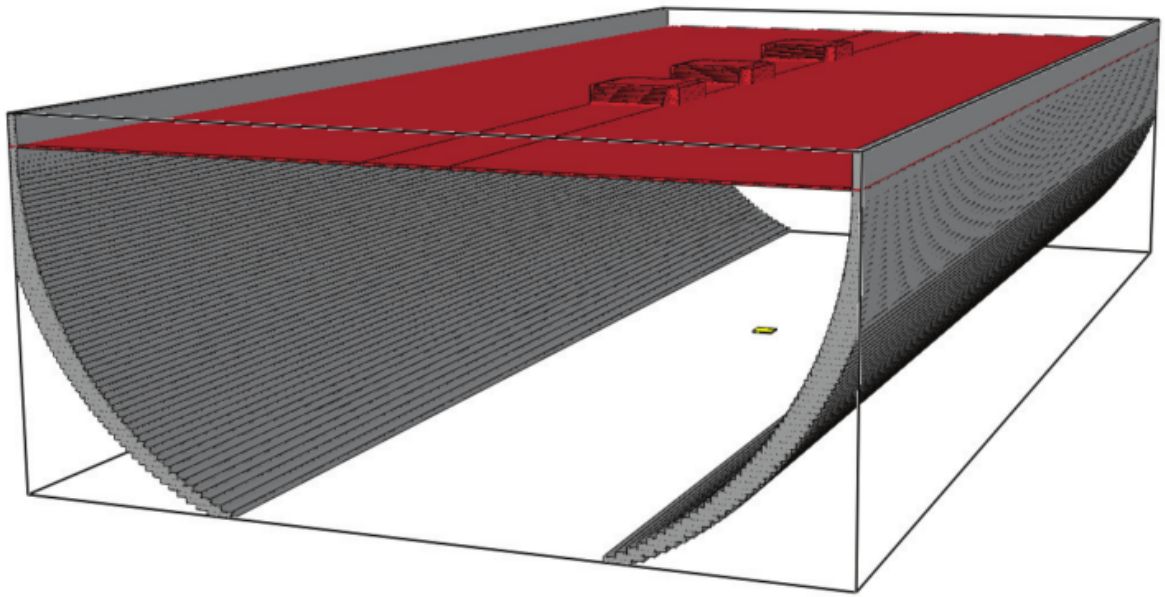

Figure: B707 cargo hold geometry.

Fire-induced fluid dynamics

- Detailed simulation of the combustion process is expensive and unnecessary; the large scale dynamics are primarily determined by the amount of heat release, its position, and the geometry.
- Commonly used models apply a heat source and input of reaction products (CO, CO2, etc.)

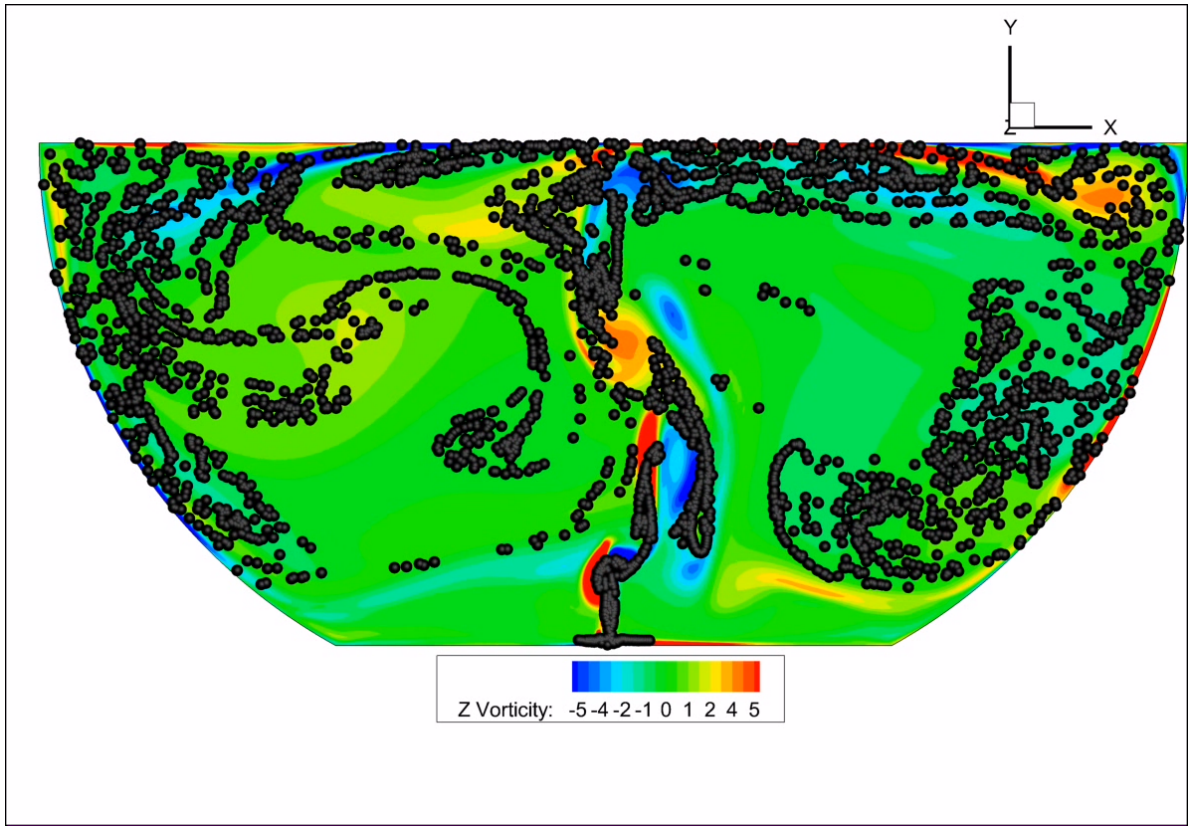

Figure: Flow driven by an enclosed heat source.

Cluttered geometry 2D

- A real fire is unlikely to happen in an empty cargo hold.
- Including some obstructions changes the flowfield considerably.

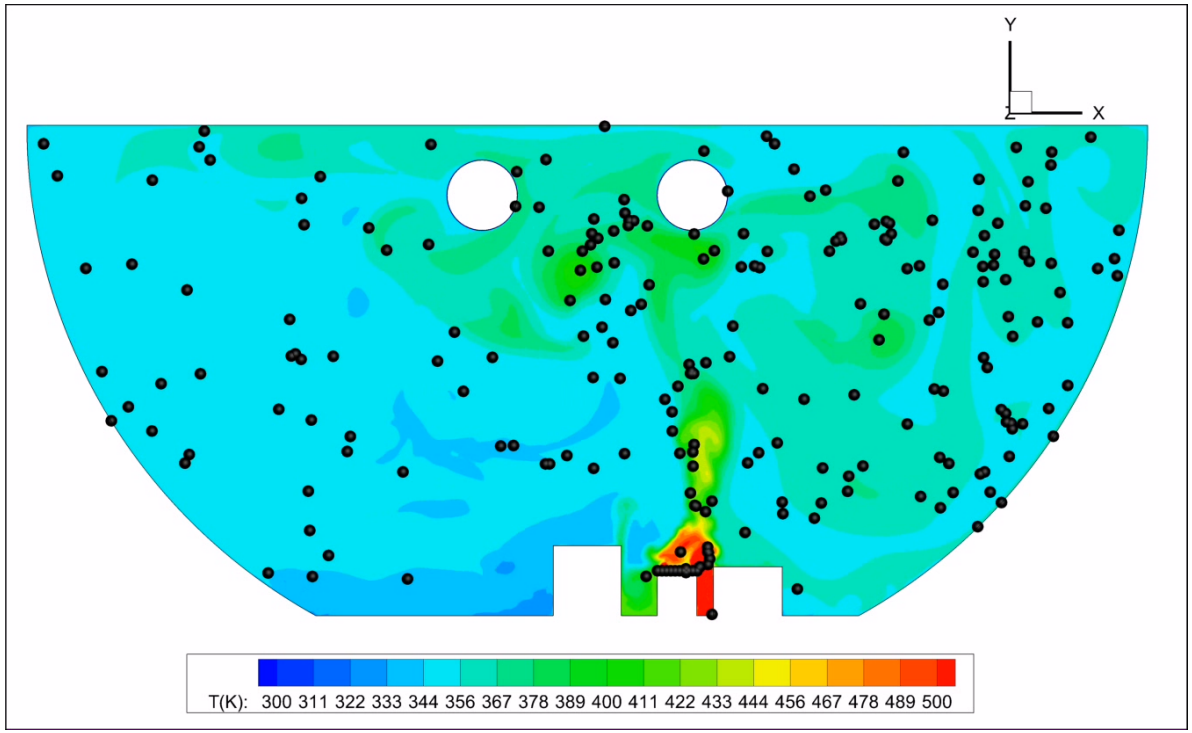

Figure: $t = 20s$ after ignition.

Simulation challenges

Simulating a single fire case is relatively straightforward, but of limited utility. There are several uncertainties to address:

- Initial position, size, and strength of a fire is unknown.
- Cargo hold geometry varies considerably depending on contents.

Simulation needs:

- Complex geometries: must handle complex boundary conditions accurately.
- Fast: uncertainty quantification will require a large number of simulations.
- Accurate: must accurately simulate vorticity-dominated turbulent flows for transport prediction.

Available tools

FDS: NIST's Fire Dynamics Simulator.

- Pros:
  - Purpose-built for smoke and heat transport from fires using large eddy simulation.
  - Combustion and radiation models.
  - Built-in post-processing tools related to smoke transport.
- Cons:
  - Handles complex boundaries with Cartesian cut cells: inaccurate for anything but rectangles.

OpenFOAM

- Pros:
  - Similar combustion and radiation models to FDS, with additional thermodynamic models.
  - Handles arbitrary body-fitted meshes.
  - Wide array of LES models.
- Cons:
  - Very slow for large cases.

Fluent

- Pros:
  - Well known, full combustion and radiation modeling.
  - Handles arbitrary body-fitted meshes.
  - Wide array of LES models.
- Cons:
  - Commercial

All limited to $O(\Delta x^2)$ accuracy.

High order accurate CFD

- Even very low intensity fires will have very complex flow phenomena poorly captured by low-order CFD methods.

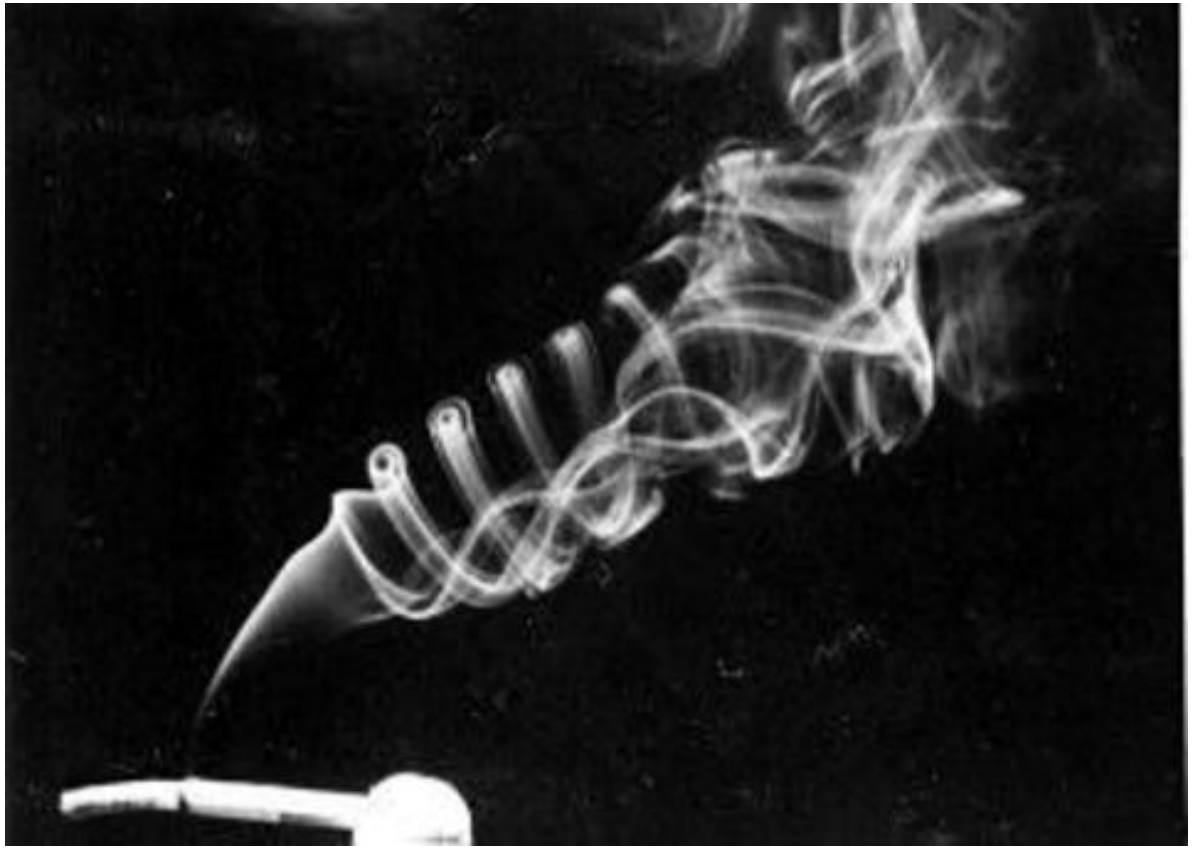

Figure: Instability of smoke from a cigarette, *Perry & Lim, 1978*

High order accurate CFD

Order of accuracy in finite differences:

$$\begin{aligned}
\frac{du}{dx} &\approx \frac{u(x+\Delta x)-u(x)}{\Delta x} + O(\Delta x) \\
\frac{du}{dx} &\approx \frac{u(x)-u(x-\Delta x)}{\Delta x} + O(\Delta x) \\
\frac{du}{dx} &\approx \frac{u(x+\Delta x)-u(x-\Delta x)}{2\Delta x} + O(\Delta x^2)
\end{aligned} \tag{1}$$

- Error scales like $\sim O(\Delta x^n)$ for order n.
- For a 1^{st} order method, halving the grid spacing reduces error by $\sim 1/2$.
- For a 4^{th} order method, halving the grid spacing reduces error by $\sim 1/16$.

High order accurate CFD

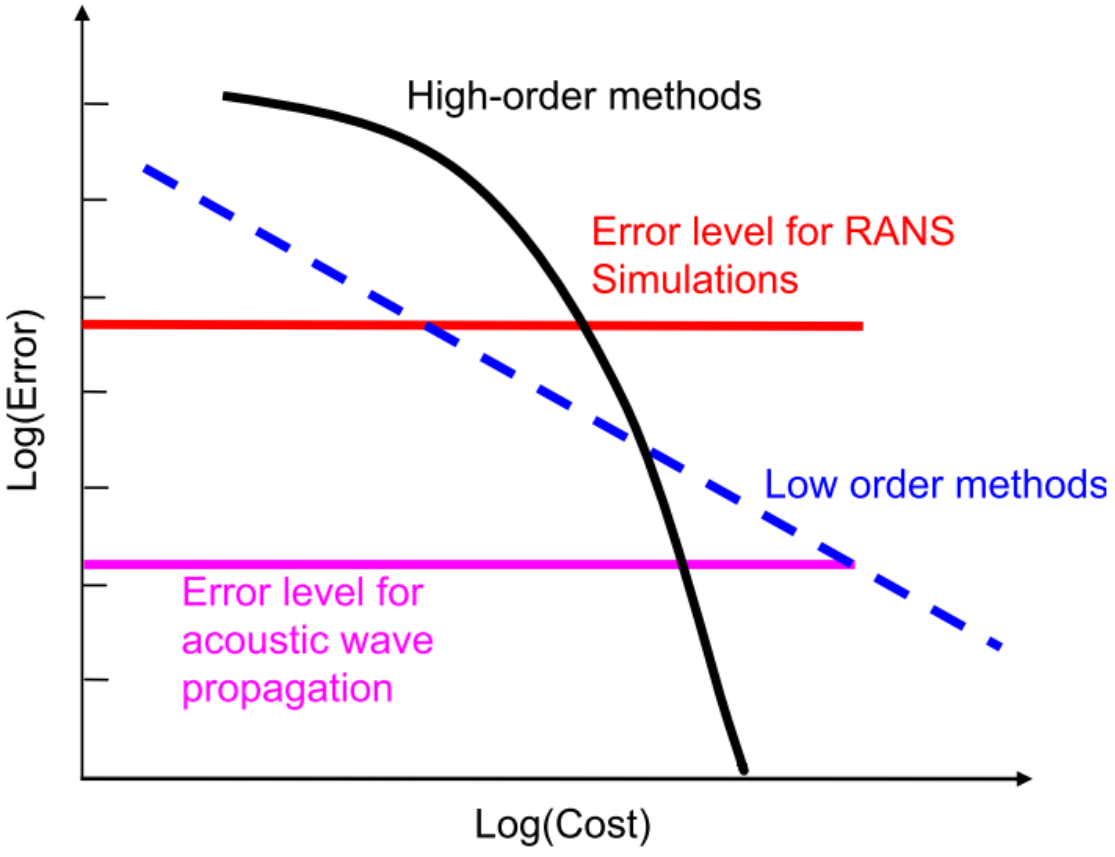

Figure: Generic error vs cost plot, *Wang, 2007*

Discontinuous Galerkin discretization method

For a multi-dimensional conservation law

$$\frac{\partial u(\mathbf{x},t)}{\partial t} + \nabla \cdot \mathbf{f}(u(\mathbf{x},t),\mathbf{x},t) = 0 \tag{2}$$

approximate $u(\mathbf{x},t)$ by

$$u(\mathbf{x},t) \approx u_h(\mathbf{x},t) = \sum_{i=1}^{N_p} u_h(\mathbf{x}_i,t) l_i(\mathbf{x}) = \sum_{i=1}^{N_p} \hat{u}_i(t)\psi_i(\mathbf{x}) \tag{3}$$

where $l_i(\mathbf{x})$ is the multidimensional Lagrange interpolating polynomial defined by grid points $\mathbf{x}_i$, N_p is the number of nodes in the element, and $\psi_i(\mathbf{x})$ is a local polynomial basis.

- Of the two equivalent approximations here, the first is termed *nodal* and the second *modal*. i.e., u_h represents values of u at discrete nodes with a reconstruction based on Lagrange polynomials, and $\hat{u}_i$ represents modes/coefficients for reconstruction with the basis ψ_n.

Discontinuous Galerkin discretization method

Substituting the approximation u_h into the conservation law:

$$\frac{\partial u_h}{\partial t} + \nabla \cdot \mathbf{f}_h = 0$$

Integrate with a test function ψ_j, the same as used to represent the polynomial above,

$$\int_V \frac{\partial u_h}{\partial t} \psi_j \, dV + \int_V \nabla \cdot \mathbf{f}_h \psi_j \, dV = 0$$

Integration by parts on the spatial component:

$$\int_V \frac{\partial u_h}{\partial t} \psi_j \, dV - \int_V \nabla \psi_j \cdot \mathbf{f}_h \, dV + \oint_S \psi_j \mathbf{f}^\star{}_h \cdot \mathbf{n} \, dS = 0$$

Using the modal representation, $u_h = \sum_{i=1}^{N_p} \hat{u}_i(t) \psi_i(\mathbf{x})$

$$\int_V \frac{\partial \hat{u}_i \psi_i}{\partial t} \psi_j \, dV - \int_V \nabla \psi_j \cdot \hat{\mathbf{f}}_i \psi_i \, dV + \oint_S \psi_j \hat{\mathbf{f}}_i^\star \psi_i \cdot \mathbf{n} \, dS = 0$$

which gives the semi-discrete form of the classic modal DG method,

$$\hat{\mathbf{M}}_{ij} \frac{d\hat{u}_i}{dt} = \int_V \nabla \psi_j \cdot \hat{\mathbf{f}}_i \psi_i \, dV + \oint_S \psi_j \hat{\mathbf{f}}_i^\star \phi_i \cdot \mathbf{n} \, dS$$

Here $\mathbf{M}$ is the *mass matrix* (identity for orthonormal bases), $\mathbf{n}$ the vector normal at an element surface, and $\hat{\mathbf{f}}^\star$ is a conservative flux function at interfaces, equivalent to that used in finite volume methods.

Discontinuous Galerkin discretization method

The modal coefficients $\hat{\mathbf{u}}$ can always be represented on nodal locations $\mathbf{u}$ through a change of basis by the *Vandermonde matrix*,

$$V\hat{\mathbf{u}} = \mathbf{u}$$

which turns the previous modal method into a nodal method. This code uses unstructured tetrahedral elements in 3D with Legendre-Gauss-Lobatto nodes:

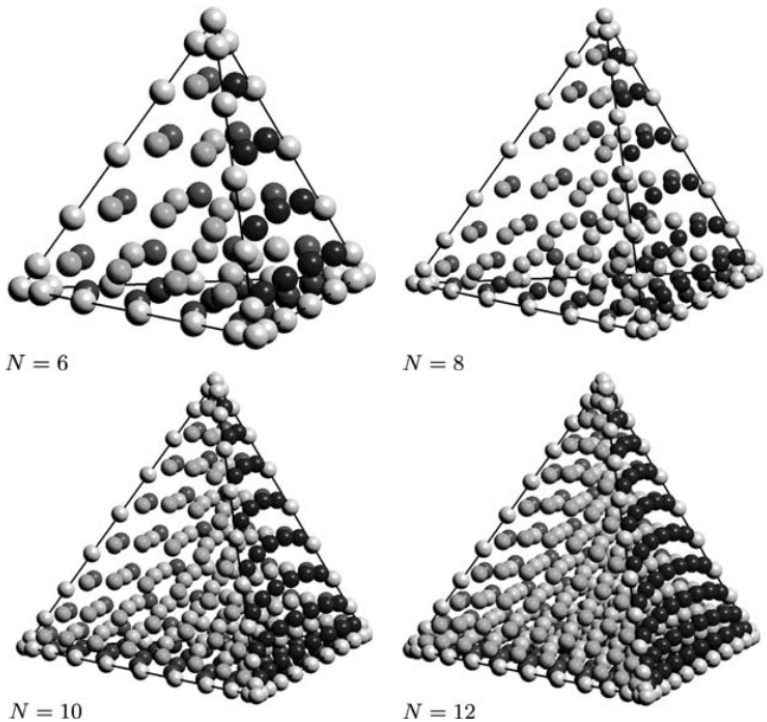

(a) Volume nodes for varying order, Hesthaven & Warburton.

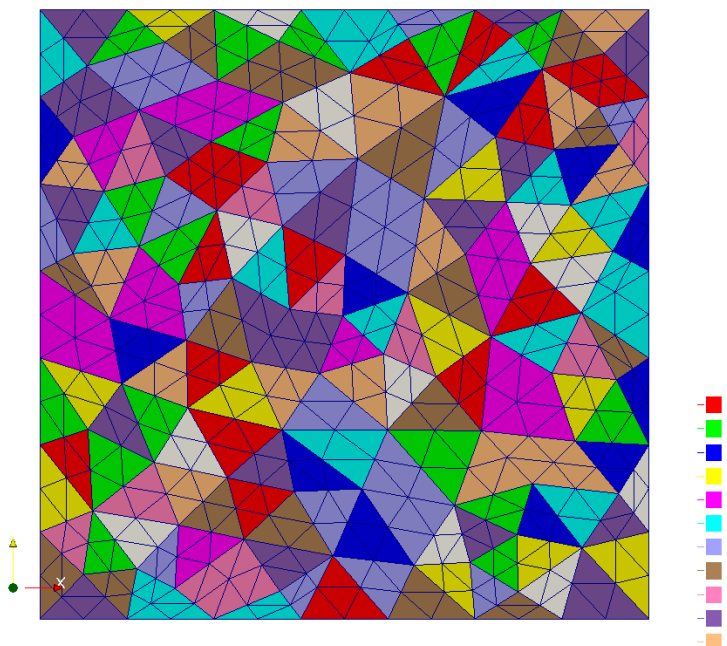

(b) $N = 2$ element surfaces; nodes are at line intersections.

Discretization method - solving the discretized equations

This ends up with a potentially very large system of ODEs to be solved:

$$\frac{d\mathbf{u}}{dt} = \mathbf{f}(\mathbf{u}, \mathbf{u}', \mathbf{t})$$

Simplest method for integrating this system in time is the explicit (forward) Euler method:

$$\mathbf{u}^{n+1} = \mathbf{u}^n + \Delta t \mathbf{f}(\mathbf{u}, \mathbf{u}', \mathbf{t})^{\mathbf{n}}$$

Unfortunately, explicit time-stepping for high-order DG is stable only for excessively small Δt,

$$\Delta t = O(\frac{\Delta x}{N^2})$$

where a mesh cell Δx can be very small (boundary layers, small geometric features) and N^2 quickly grows large. For any engineering-scale problem, explicit methods are unfeasible for use.

- This requires the use of implicit time-stepping methods, e.g. 1st order backward Euler:

$$\mathbf{u}^{n+1} = \mathbf{u}^n + \Delta t \mathbf{f}(\mathbf{u}, \mathbf{u}', \mathbf{t})^{\mathbf{n+1}}$$

where we now have a set of non-linear equations to solve for u^{n+1}. Typically we use 3rd order or higher time-accurate schemes.

Discretization method - solving the discretized equations

Task is to solve the very large non-linear system at each time step:

$$\mathbf{F}(\mathbf{u}) = 0$$

Newton's method for this problem derives from a Taylor expansion (Knoll/Keyes 2004):

$$\mathbf{F}(\mathbf{u}^{k+1}) = \mathbf{F}(\mathbf{u}^k) + \mathbf{F}'(\mathbf{u}^k)(\mathbf{u}^{k+1} - \mathbf{u}^k)$$

resulting in a sequence of linear systems

$$\mathbf{J}(\mathbf{u}^k)\delta\mathbf{u}^k = -\mathbf{F}(\mathbf{u}^k), \quad \mathbf{u}^{k+1} = \mathbf{u}^k + \delta\mathbf{u}^k$$

for the Jacobian $\mathbf{J}$.

- The linear system $\mathbf{J}(\mathbf{u}^k)\delta\mathbf{u}^k = -\mathbf{F}(\mathbf{u}^k)$ is straighforward enough to write, but for these methods $\mathbf{J}$ is a very large sparse matrix which is prohibitively expensive to actually compute and store.
- A mesh of 100,000 4th order cells requires roughly 250GB of memory to store in 64-bit floats.

Discretization method - solving the discretized equations

- A remedy for this is to use a "Jacobian-Free" method based on Krylov subspace iterations (e.g. GMRES, BiCGSTAB), which only require the action of the jacobian in the form of matrix-vector products:

$$\mathbf{K} = \text{span}(\mathbf{J}\delta\mathbf{r}, \mathbf{J}^2\delta\mathbf{r}, \mathbf{J}^3\delta\mathbf{r}, ...)$$

which can be approximated by a finite difference:

$$\mathbf{Jv} \approx [\mathbf{F}(\mathbf{u} + \epsilon\mathbf{v}) - \mathbf{F}(\mathbf{v})]/\epsilon$$

- This enables a solution method for the non-linear system that doesn't require ever explicitly forming the Jacobian, and instead only requires the evaluation of the RHS of the ODE.
- This is the *Jacobian-free Newton-Krylov* (JFNK) method:
  - Take a Newton step from the previous iterate.
  - Approximately solve the linear system using a matrix-free Krylov method.
  - Repeat until desired convergence is reached, and move to the next physical time step.
- Current solver uses a damped Newton line-search for the non-linear systems coupled with a GMRES Krylov method for the linear systems.

1D test case

1D Poisson test case to illustrate accuracy vs computational cost:

$$\frac{d^2u}{dx^2} = -20 + a\phi'' \cos\phi - a\phi'^2 \sin\phi \qquad (4)$$

$$a = 0.5,\ \phi(x) = 20\pi x^3$$

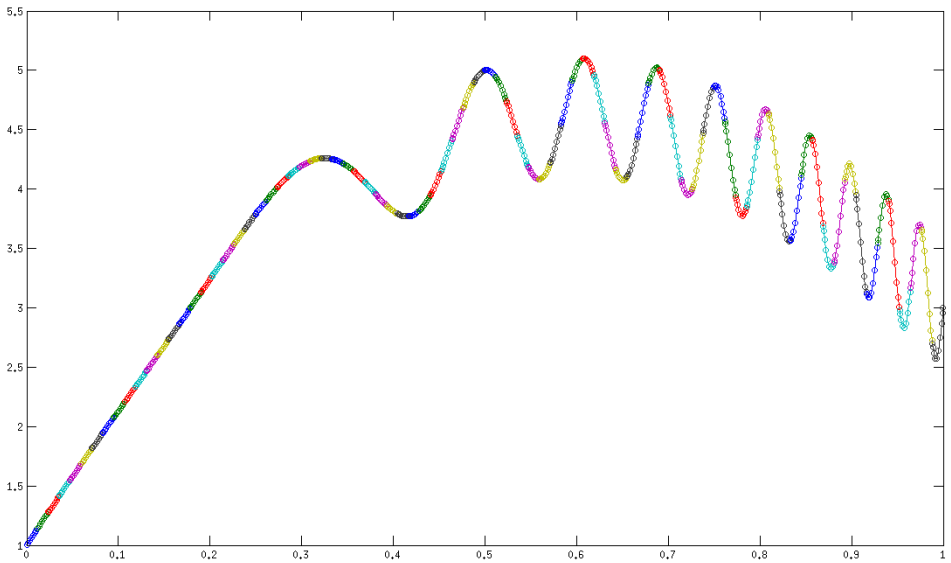

1D test case

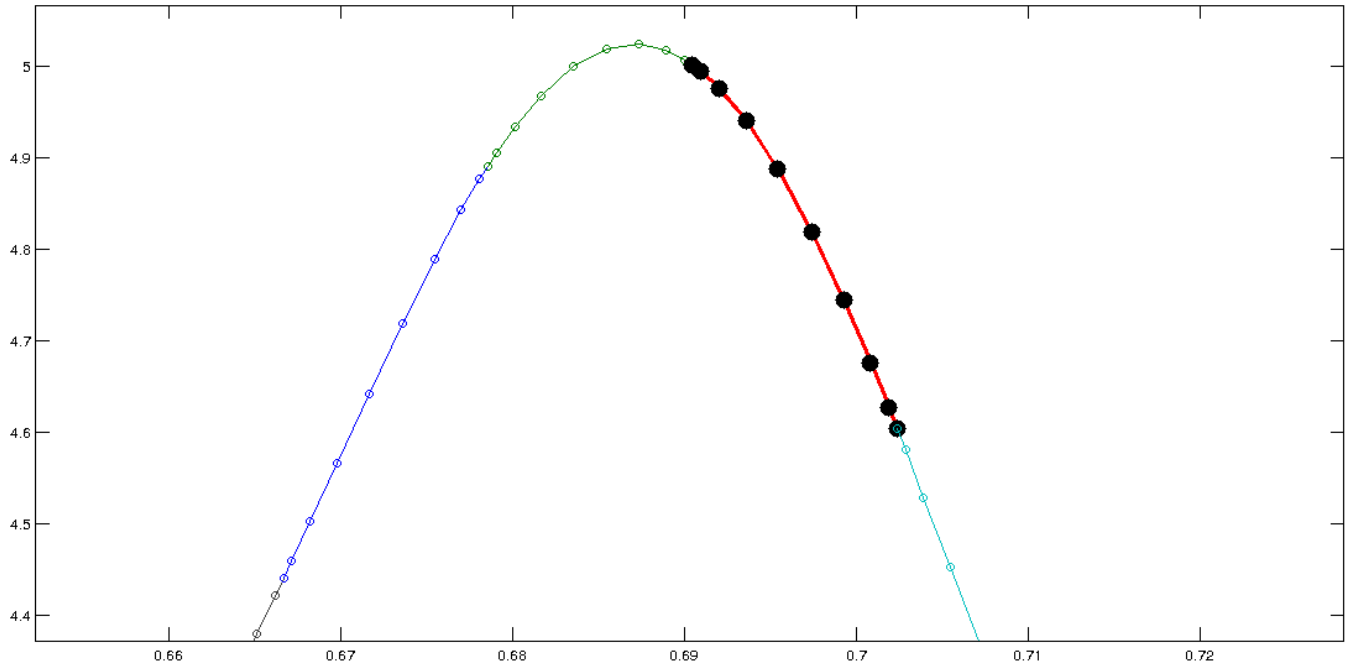

Figure: Close up of a single element with a 9th order polynomial basis.

1D test case

- For an ideal numerical method, computational cost is linearly proportional to the number of unknowns (degrees of freedom).
  - *e.g. 10 cells with 10 quadrature nodes compared to 50 cells with 2 quadrature nodes.*
- The end result is achieving equivalent accuracy with less computational expense or higher accuracy at similar computational expense compared to traditional finite volume methods.

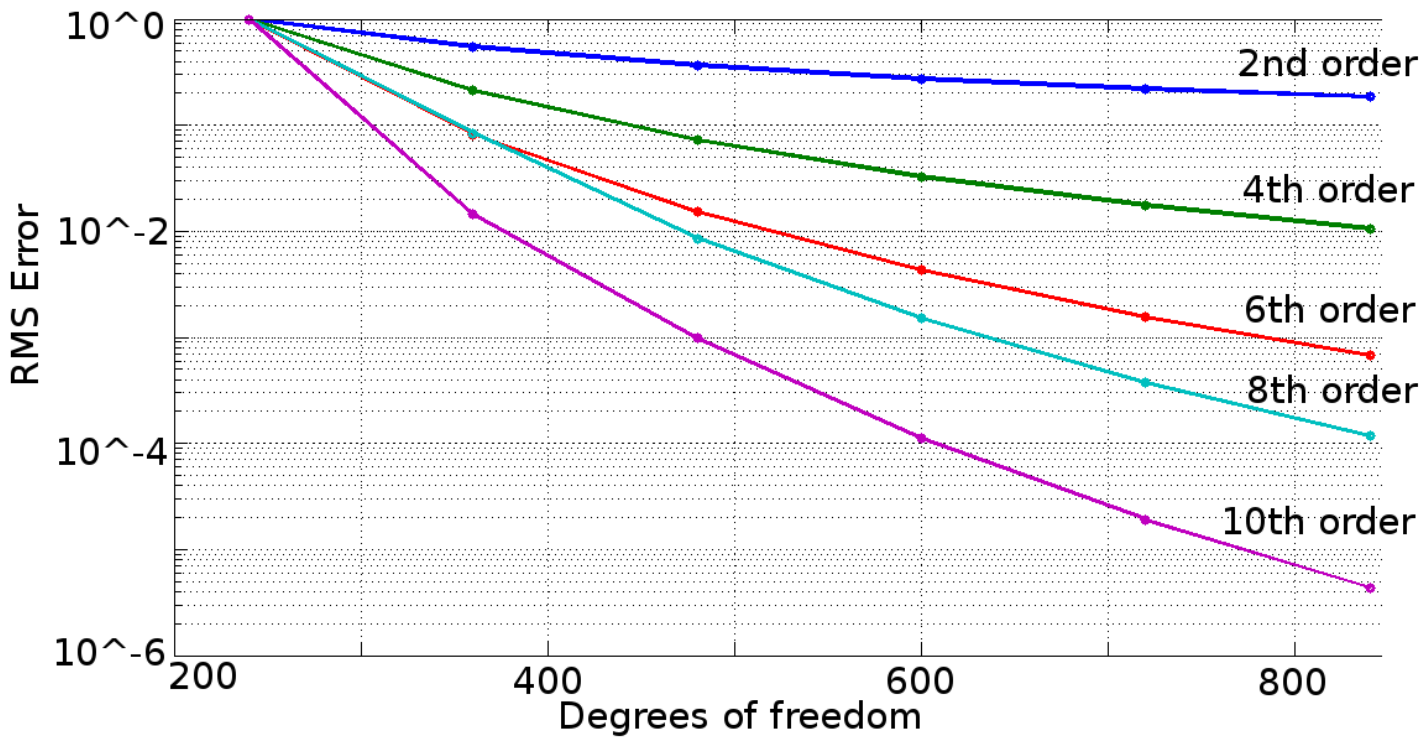

Figure: Error for varying order of accuracy with constant DOFs on 1D test case.

Test case - Isentropic vortex

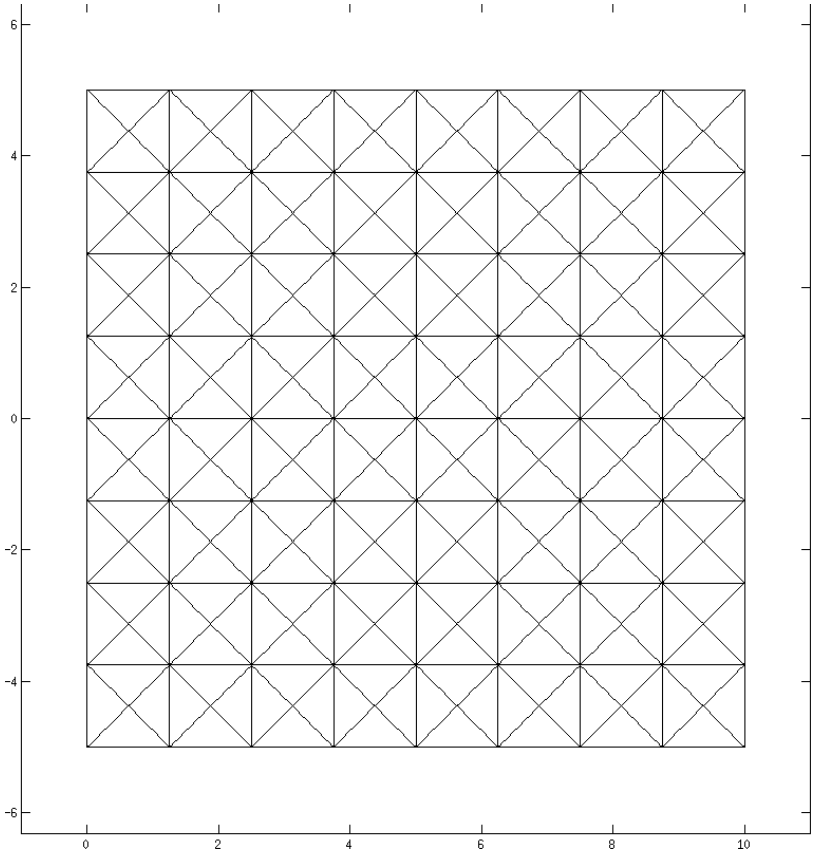

(a) Coarse mesh for vortex case.

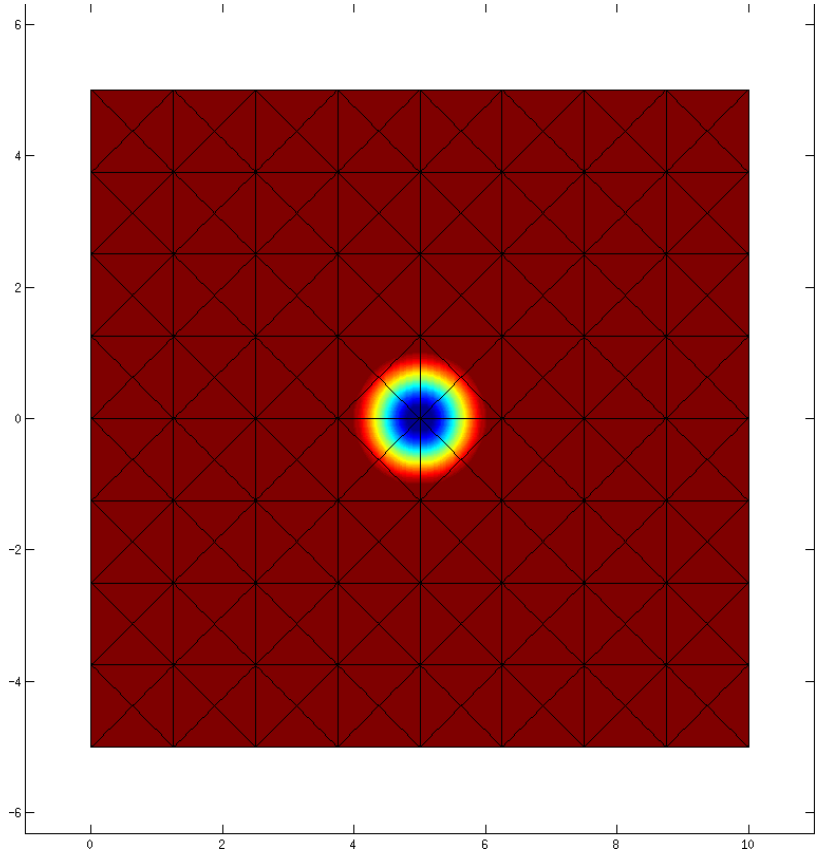

(b) Initial vorticity.

Test case - Isentropic vortex

- Non-dissipative vorticity convection is essential for these simulations.
- Test case of Yee et al (1999) for a convecting vortex is an exact solution for the compressible Euler equations. Free-stream conditions are

$$\rho = 1, u = u_\infty, v = v_\infty, p = 1$$

with an initial perturbation

$$(du, dv) = \frac{\beta}{2\pi} \exp\left(\frac{1 - r^2}{2}\right) [-(y - y_0), (x - x_0)]$$

$$T = 1 - \frac{(\gamma - 1)\beta^2}{8\gamma\pi^2} \exp(1 - r^2)$$

$$\rho = T^{\frac{1}{\gamma - 1}}$$

$$p = \rho^\gamma$$

for vortex center (x_0, y_0), and distance from center $r = \sqrt{(x - x_0)^2 + (y - y_0)^2}$.

Test case - Isentropic vortex - 1st order (c.f. 2nd order FV)

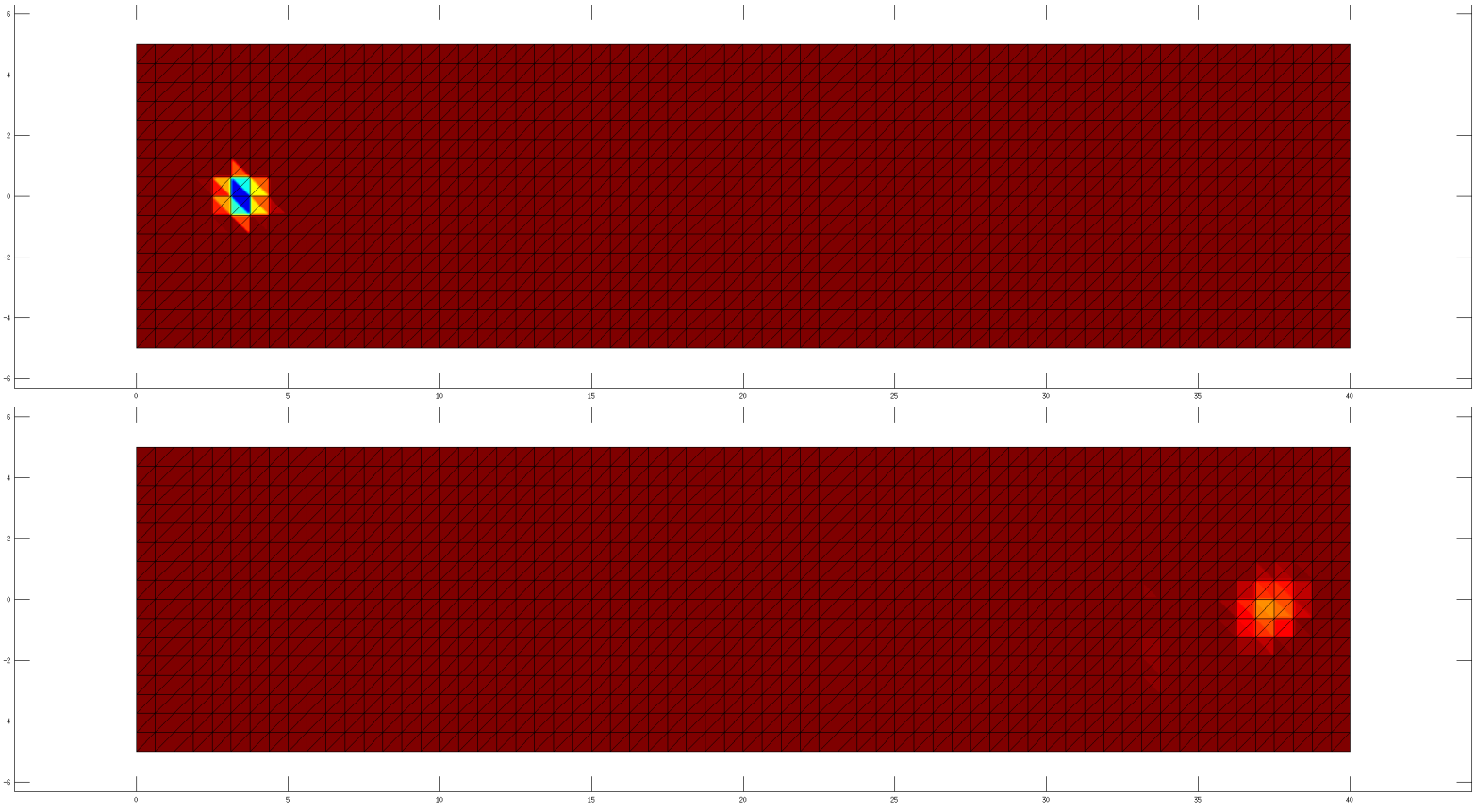

Figure: Vortex transport over 35 characteristic lengths, $O(\Delta x)$.

Test case - Isentropic vortex - 2nd order

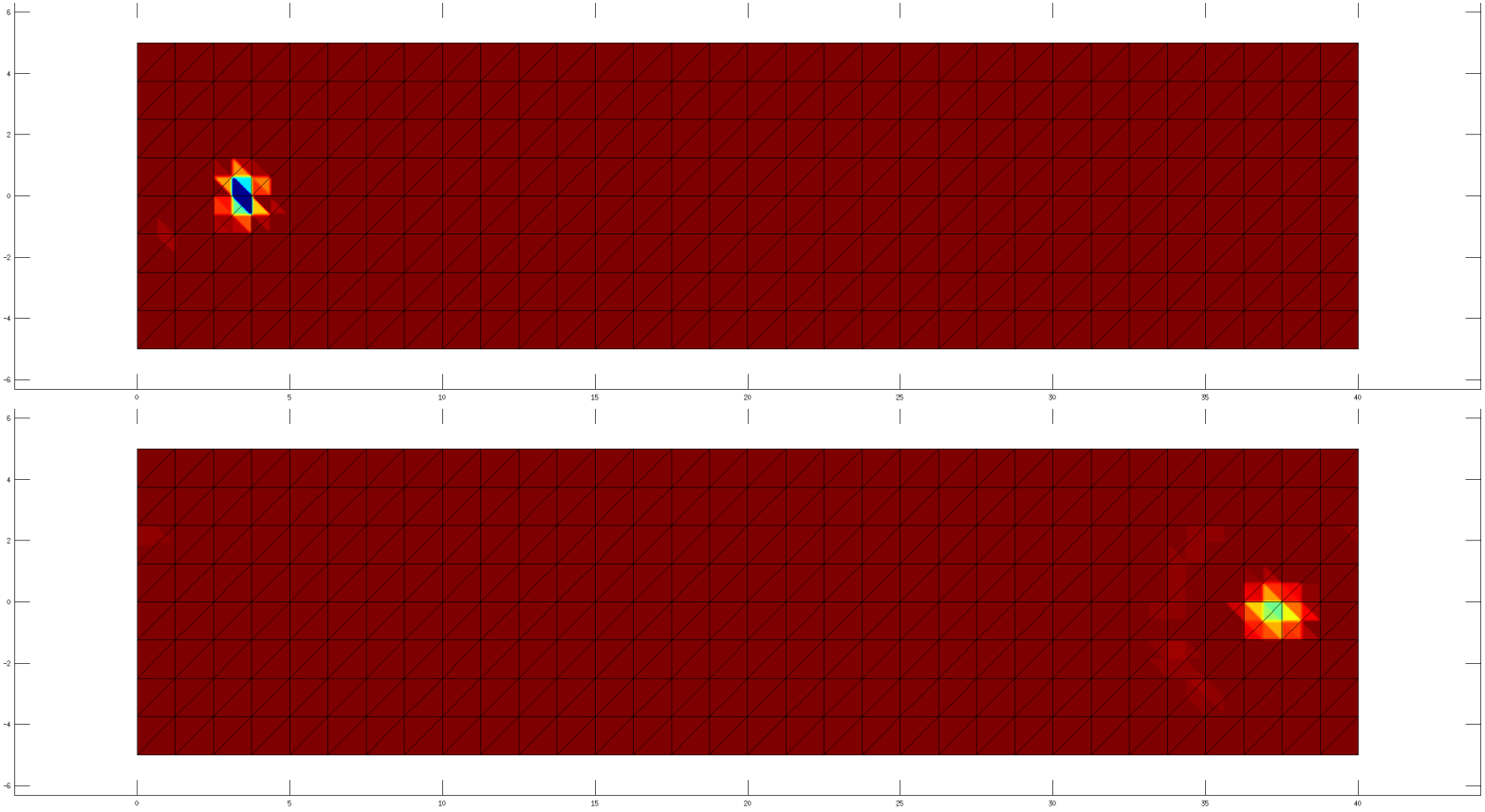

Figure: Vortex transport over 35 characteristic lengths, $O(\Delta x^2)$.

Test case - Isentropic vortex - 3rd order

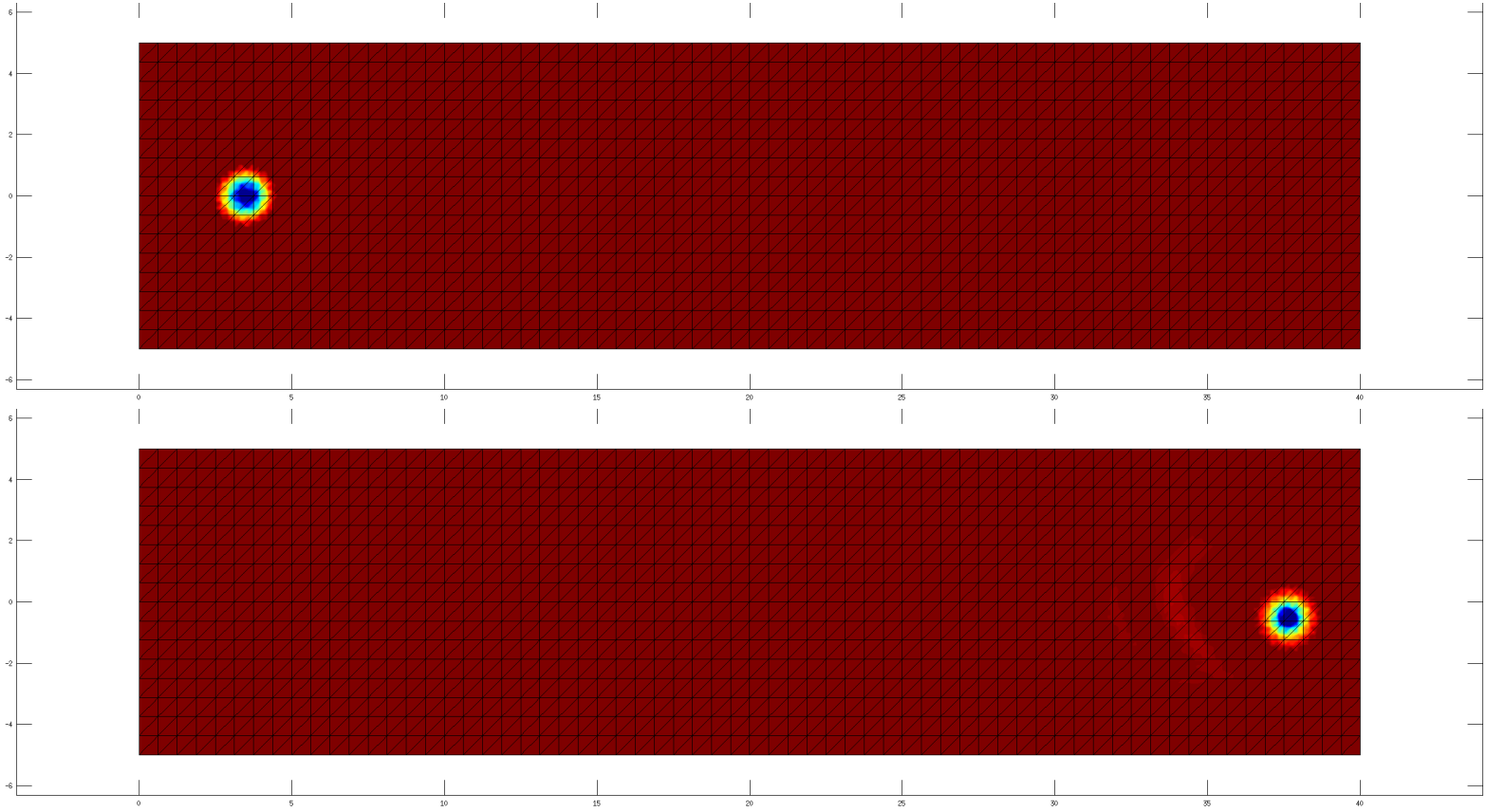

Figure: Vortex transport over 35 characteristic lengths, $O(\Delta x^3)$.

Test case - Isentropic vortex - 4th order

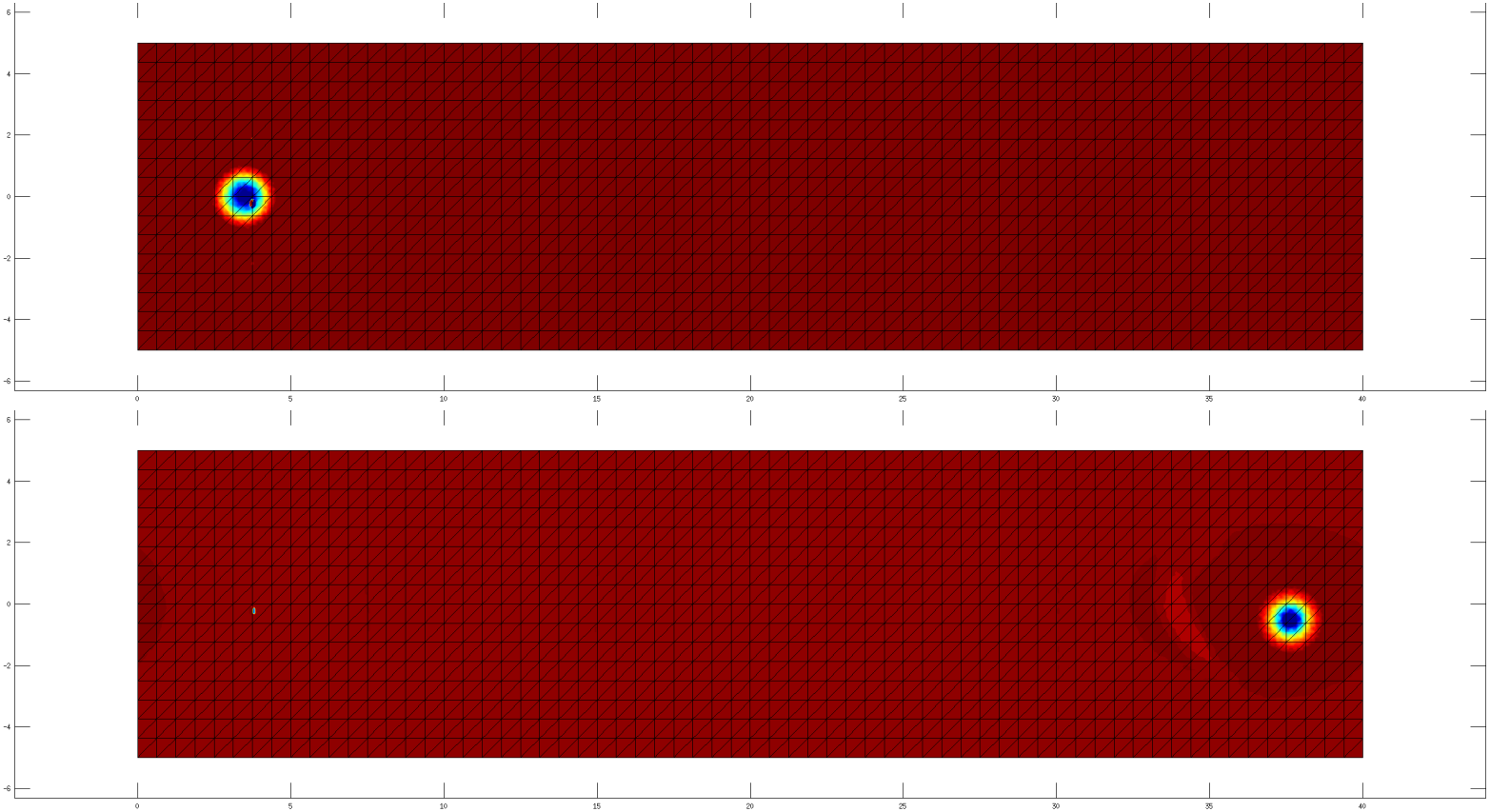

Figure: Vortex transport over 35 characteristic lengths, $O(\Delta x^4)$.

Test case - Isentropic vortex order of accuracy

- L_2 norm of kinetic energy losses for isentropic vortex convection.

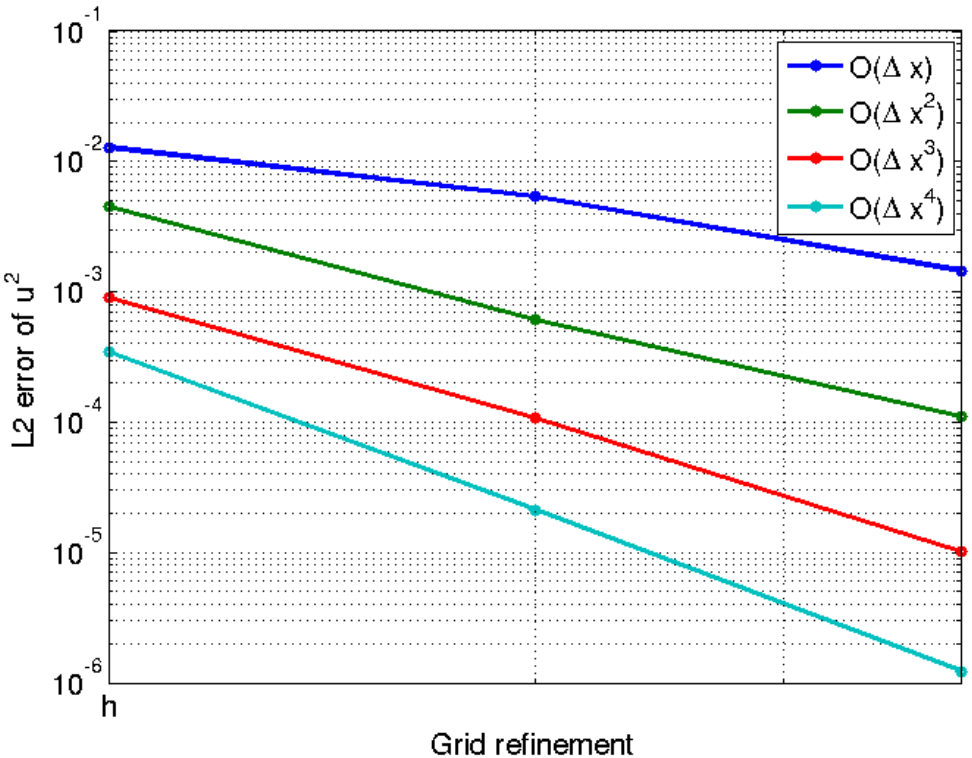

Figure: Solution accuracy versus grid refinement, for levels h, $h/2$, and $h/4$.

AIAA 2016 2D cargo hold results

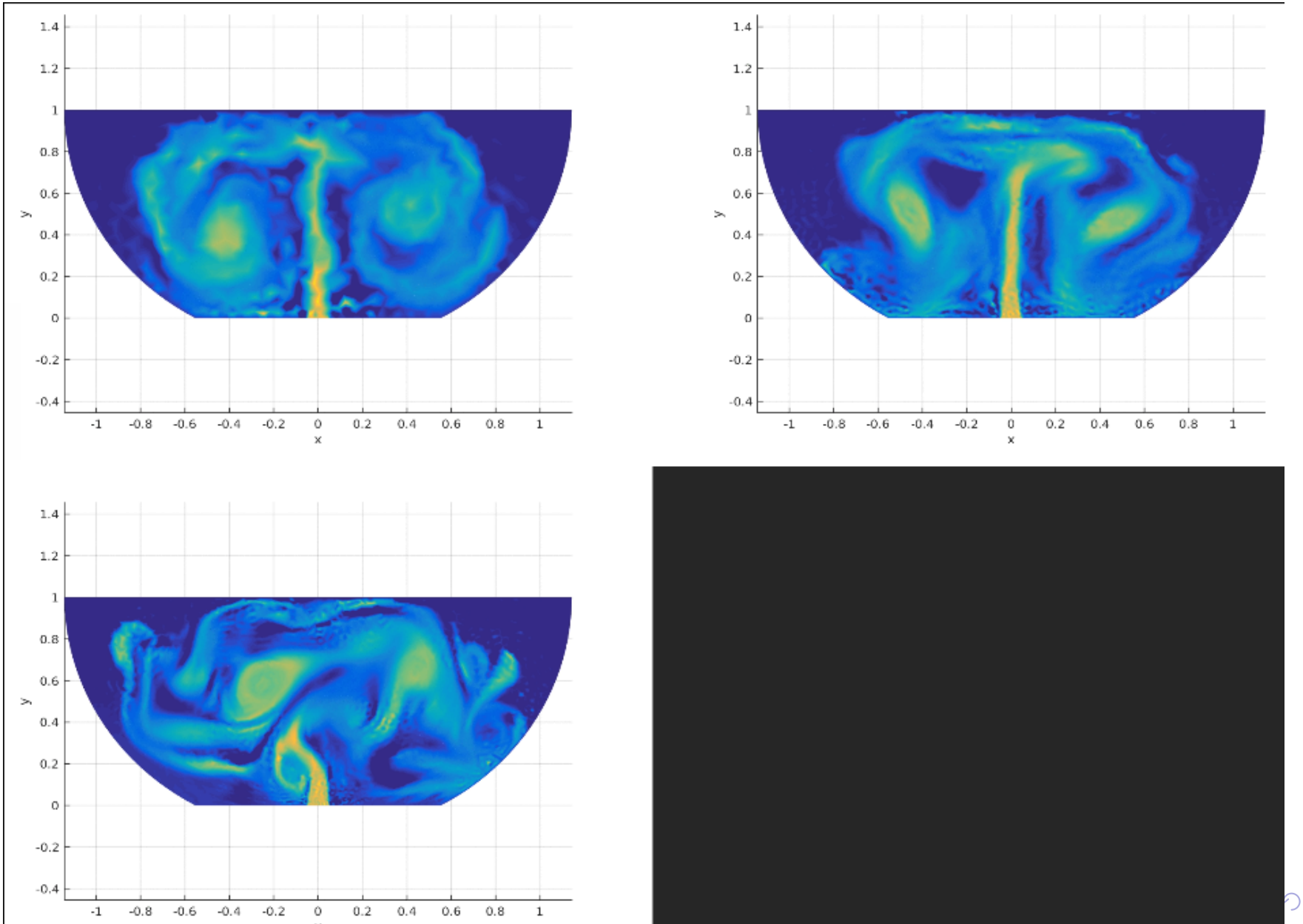

AIAA 2016 2D cargo hold results

Uncertainy Quantification for Cargo Hold Fires, DeGennaro, Lohry, Martinelli, & Rowley, *57th AIAA Structures, Structural Dynamics, and Materials Conference*, San Diego CA, Jan. 2016.

- Two objectives of this study:
  - Assess the feasibility of using DG methods for buoyancy-driven flows,
  - Use uncertainty quantification techniques to analyze statistical variations in flows.

AIAA 2016 2D cargo hold results

- The mock fire sources were chosen to vary based on 2 parameters: fire strength and location.
  - Fire location was chosen to vary between the centerline and the far right wall, exploiting the symmetry of the geometry.
  - Fire strength was chosen to vary between a weak, slowly rising plume and a faster rising plume.
- 5×5 parameter sweep performed for these 2 parameters.
- Simulations performed with 3rd order elements (10 nodes per 2D cell) with approximately 1,500 triangular cells, or 15,000 nodes. All boundary conditions are isothermal non-slip walls. Time integration by 3rd order backward difference formula (BDF).

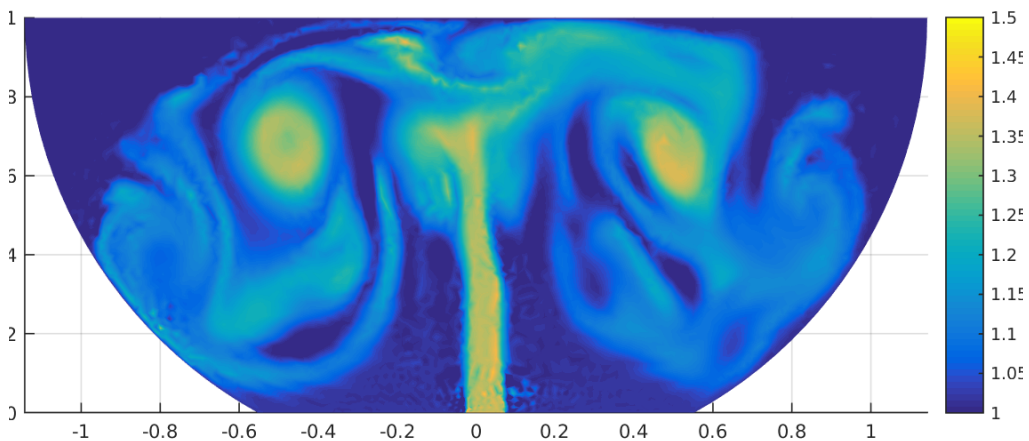

Figure: Flow driven by a heat source in a 2D cross-section. Colormap shown is temperature normalized by the initial bulk temperature.

AIAA 2016 2D cargo hold results

- Time evolution of temperature field:

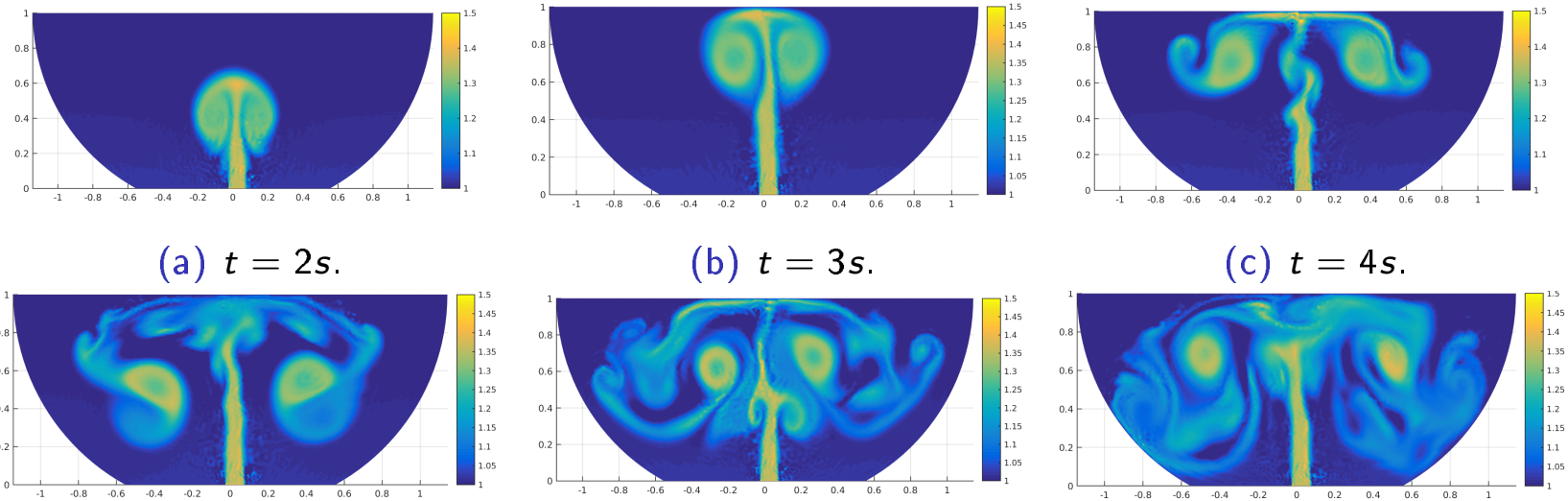

(a) $t = 2s$. (b) $t = 3s$. (c) $t = 4s$.

(d) $t = 5s$. (e) $t = 6s$. (f) $t = 7s$.

Figure: Temperature field time evolution for $T_s = 1.486$, $x_s = 0.024$ case.

AIAA 2016 2D cargo hold results

- Variation of fire source location:

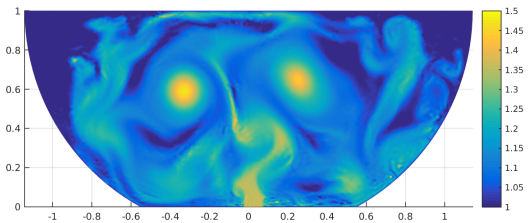

(a) $x_s = 0.024m$.

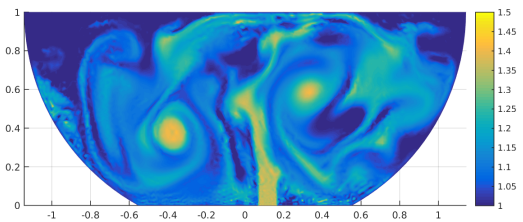

(b) $x_s = 0.116m$.

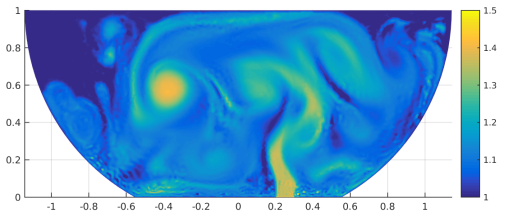

(c) $x_s = 0.262m$.

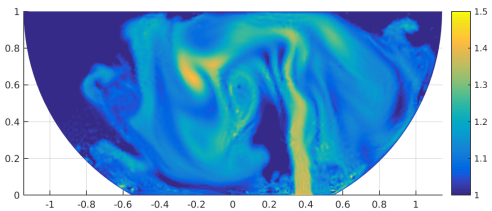

(d) $x_s = 0.387m$.

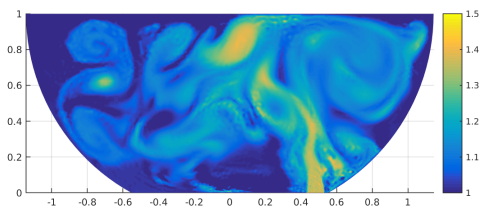

(e) $x_s = 0.480m$.

Figure: Temperature fields for $T_s = 1.486$ source at the 5 source locations, time $t = 10s$ after startup.

AIAA 2016 2D cargo hold results

- Variation of fire source temperature:

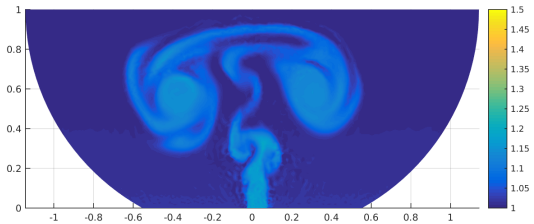

(a) $T_s = 1.214$.

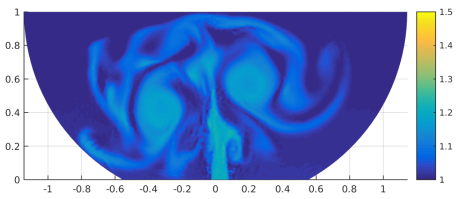

(b) $T_s = 1.269$.

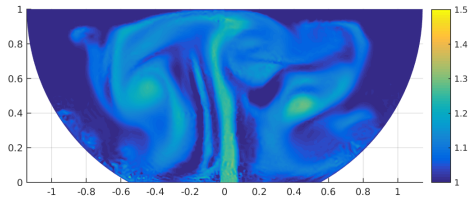

(c) $T_s = 1.350$.

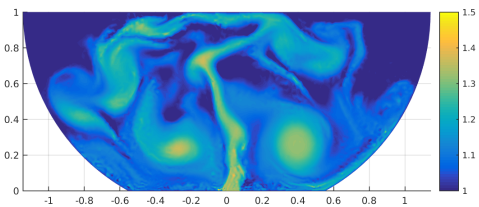

(d) $T_s = 1.431$.

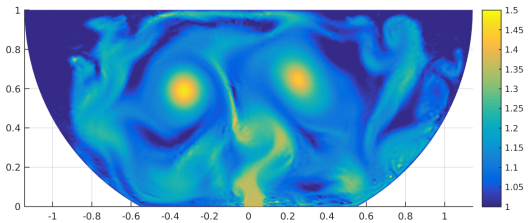

(e) $T_s = 1.486$.

Figure: Temperature fields at $x_s = 0.024m$ for the 5 values of temperature source, time $t = 10s$ after startup.

AIAA 2016 2D cargo hold results

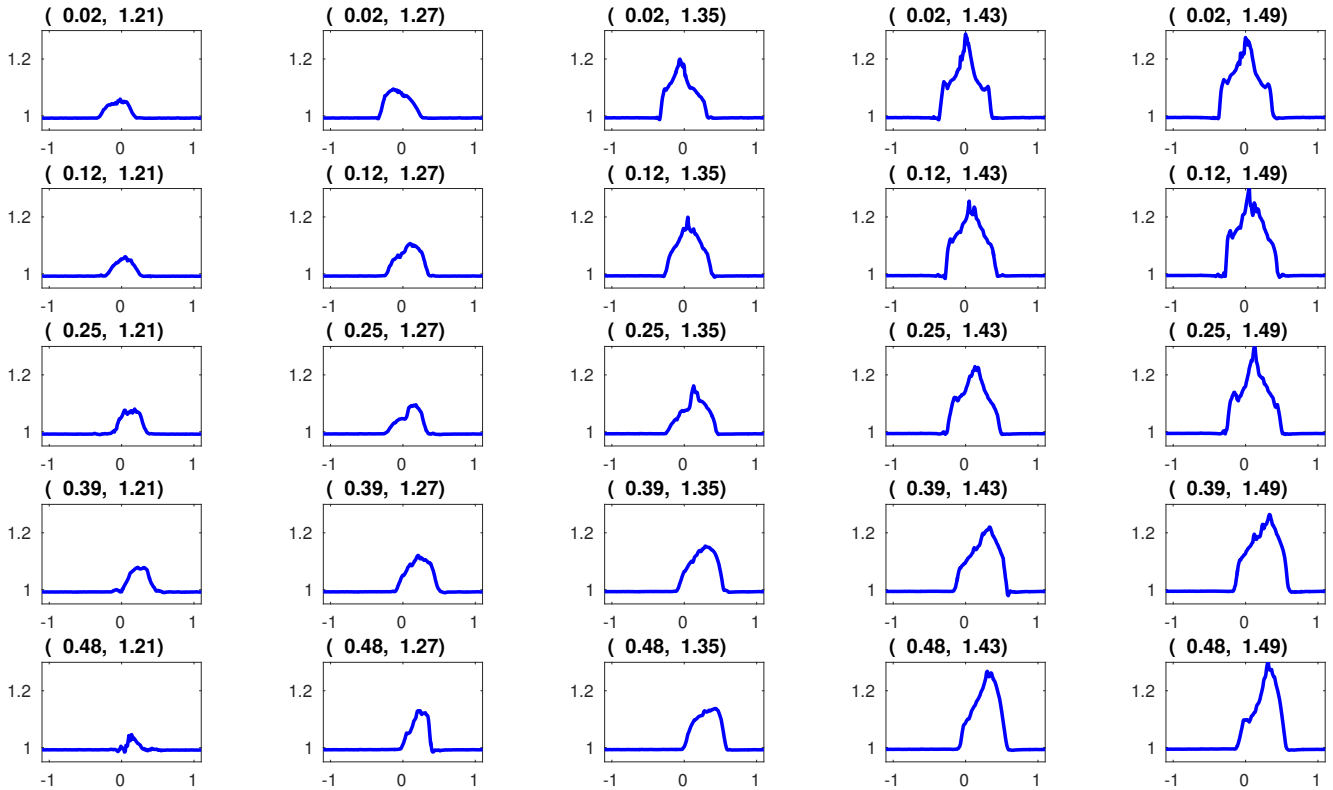

Figure: Time-averaged ceiling temperature distributions collected at the 25 quadrature nodes. Each subtitle corresponds to the parameter pair (x_S, T_S).

3D isentropic vortex

- Current work is on verification and validation of the full 3D problem.

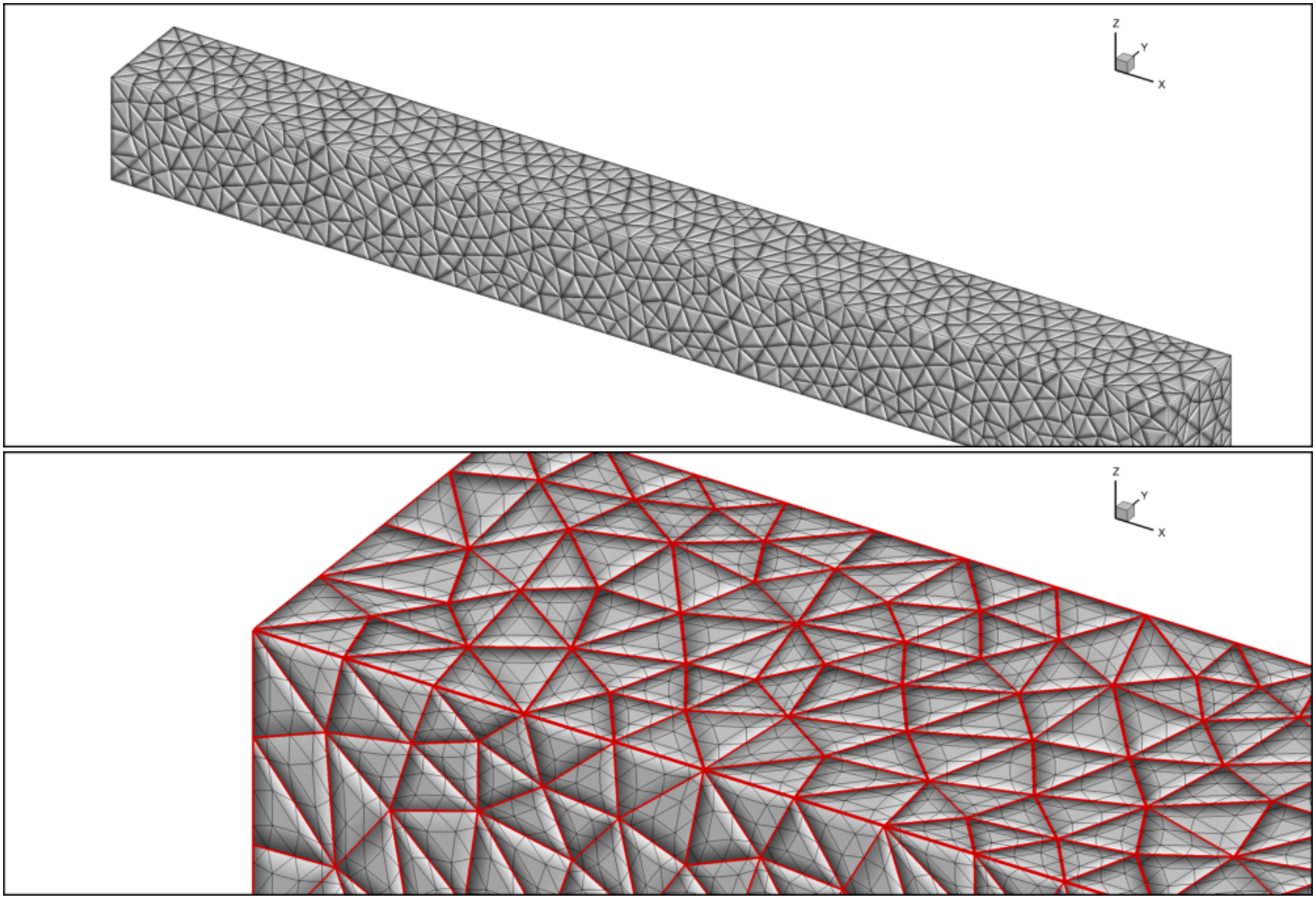

Figure: Comparison of mesh and 4th order elements.

3D isentropic vortex

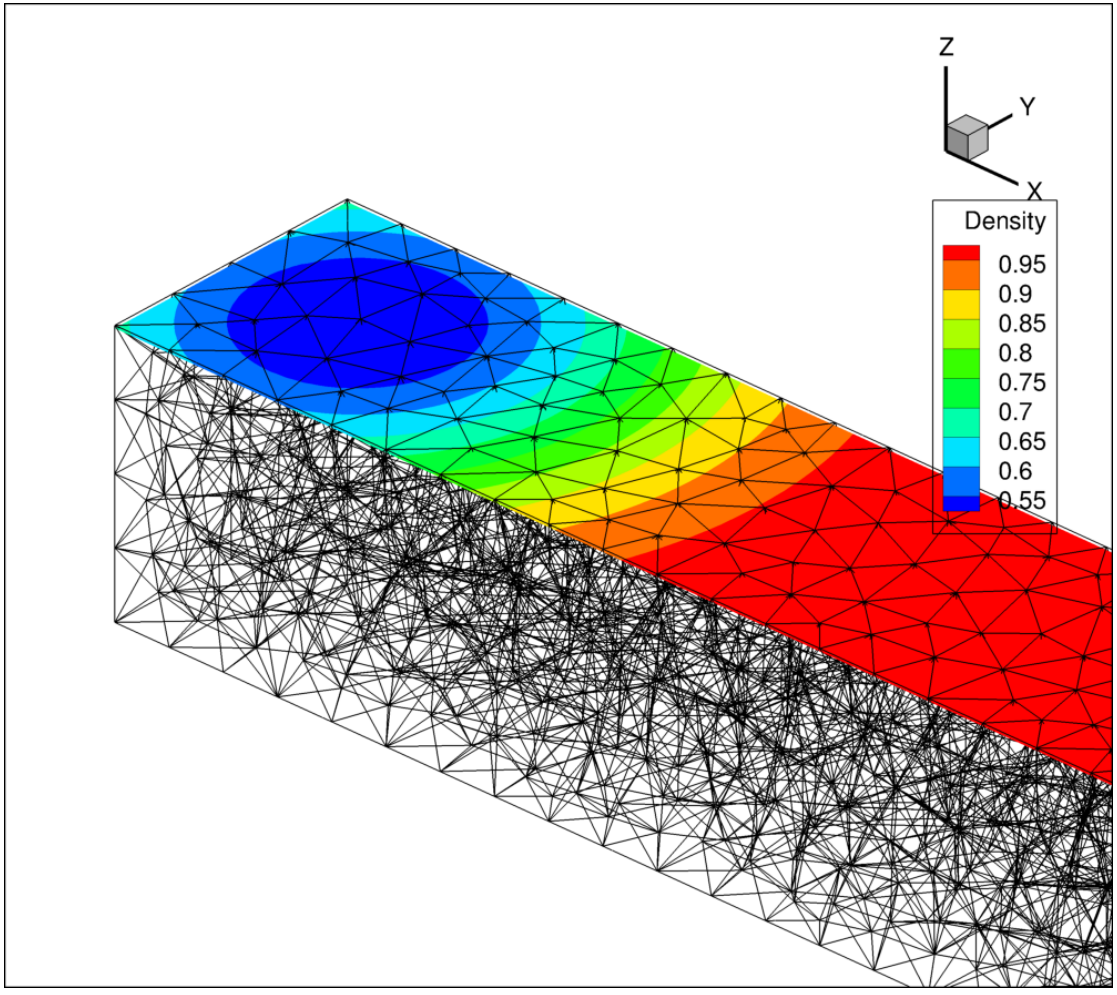

3D isentropic vortex

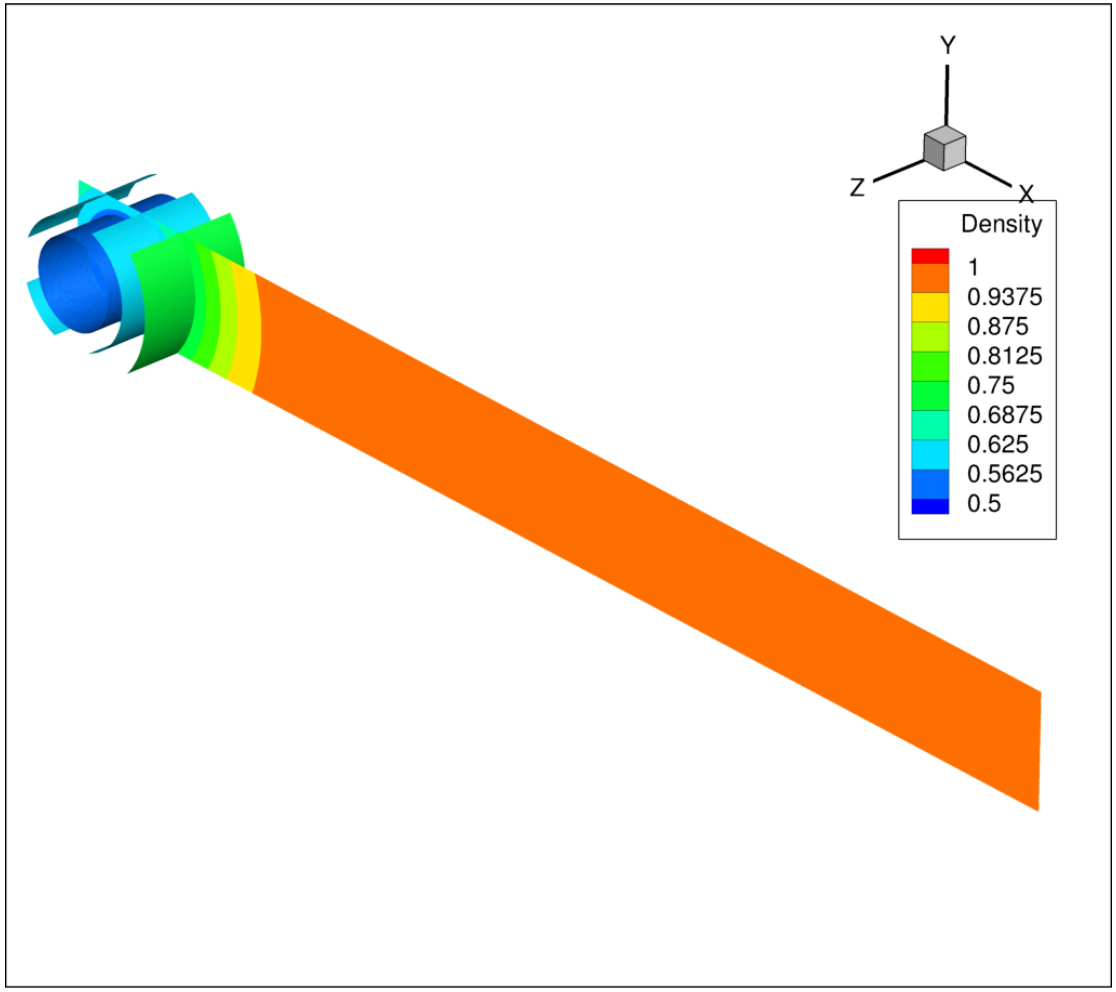

3D isentropic vortex

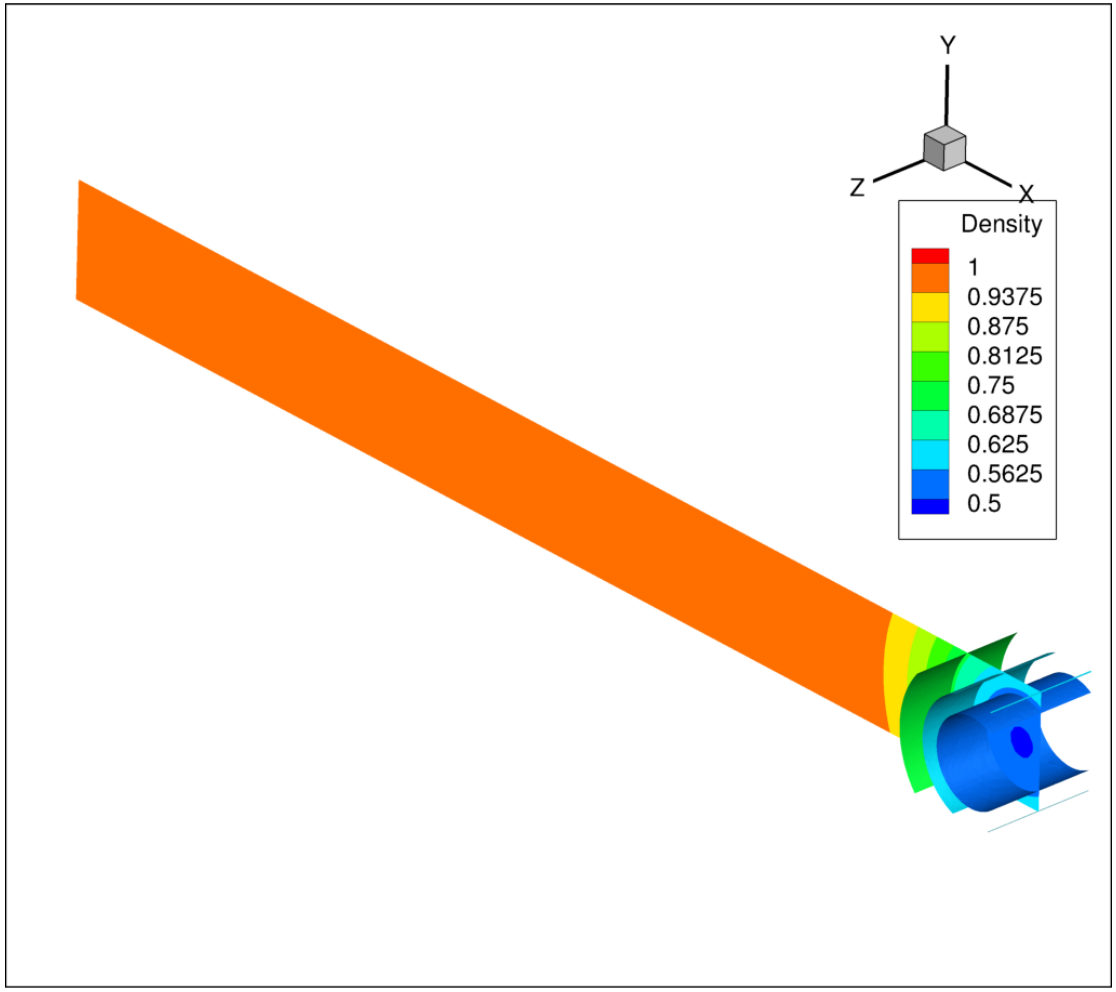

3D driven cavity

- Standard test case for viscous CFD. The "lid" of the cavity drives circulation through viscous entrainment similar to the buoyancy-driven instabilities.

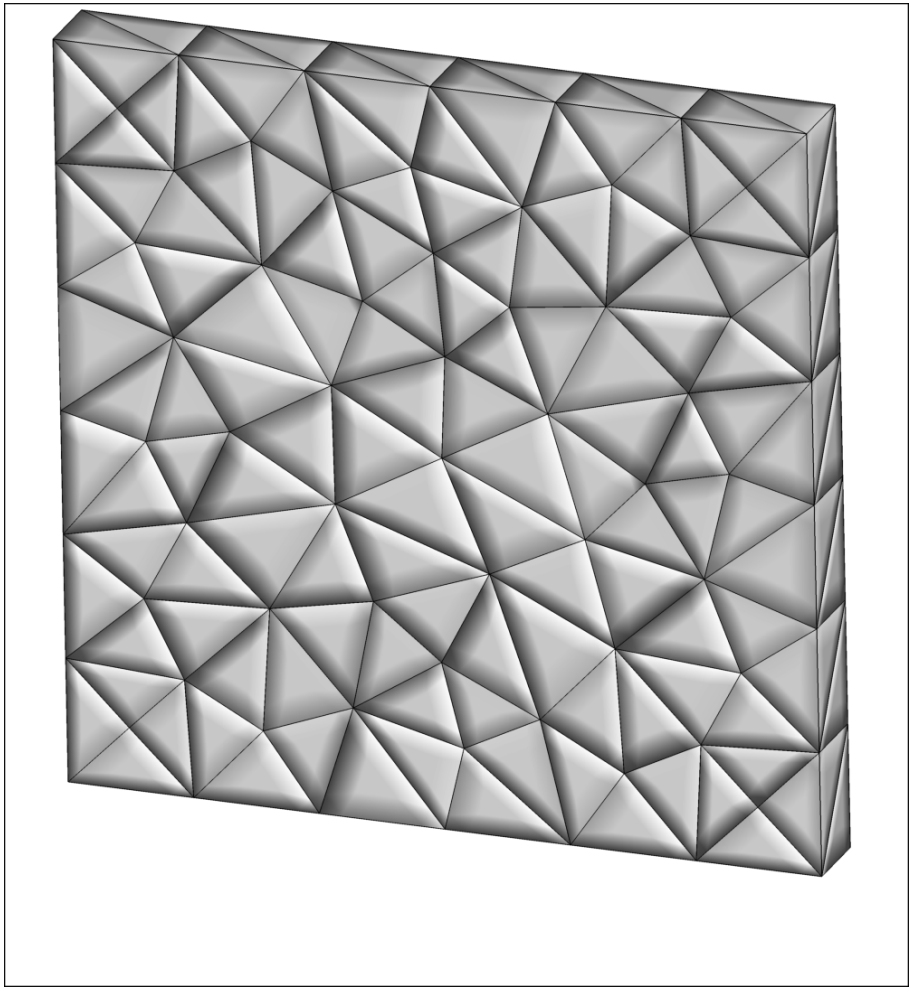

Figure: 354 cells 3D, 6x6x1 mesh.

3D driven cavity

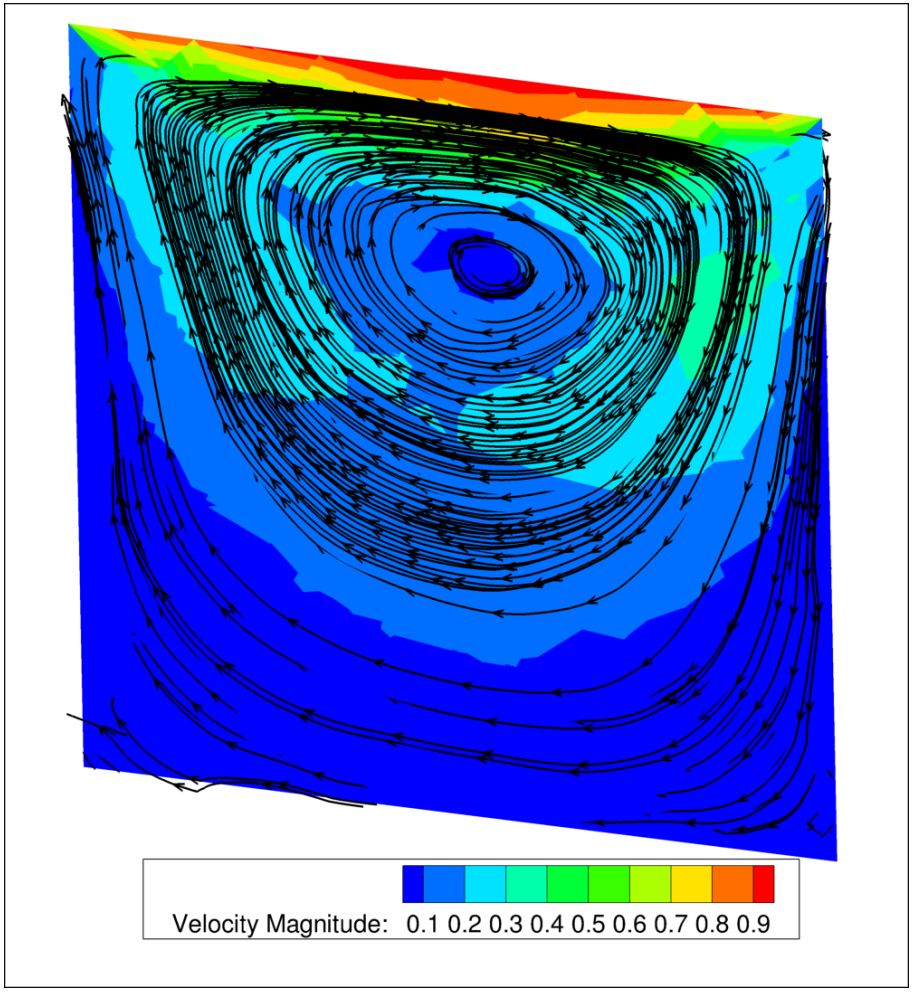

Figure: 1st order, 354 cells.

3D driven cavity

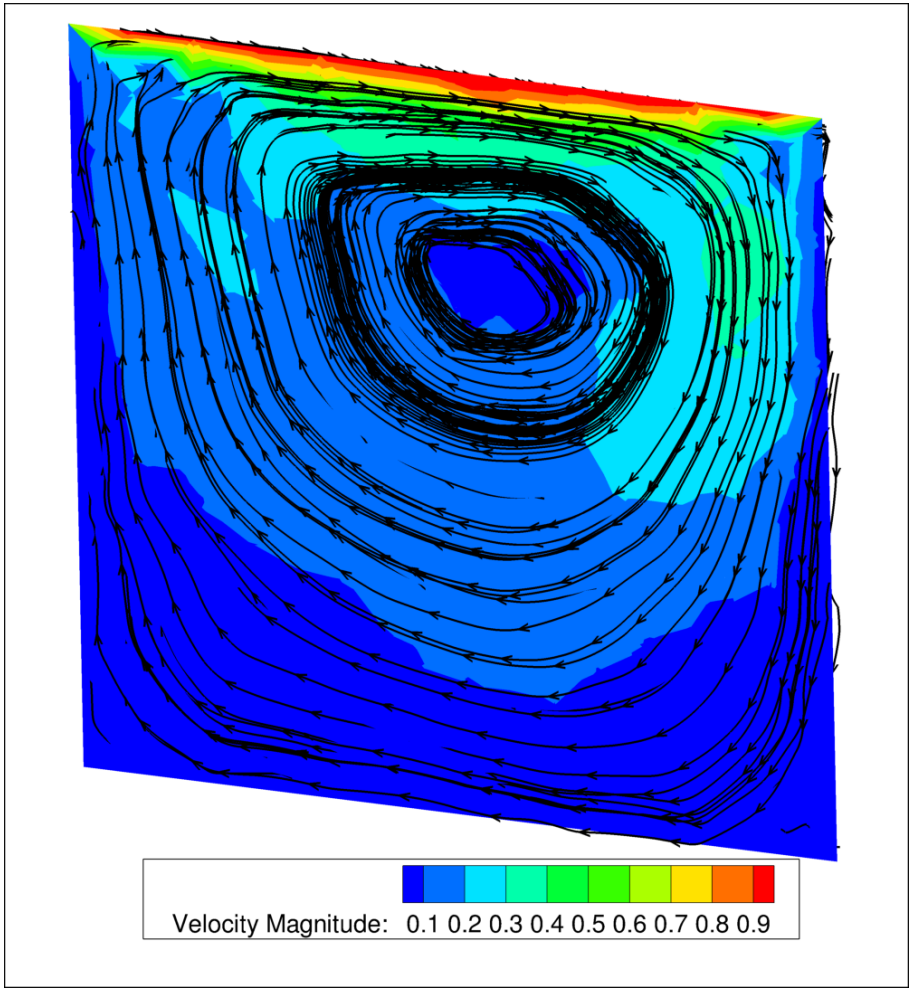

Figure: 2nd order, 354 cells.

3D driven cavity

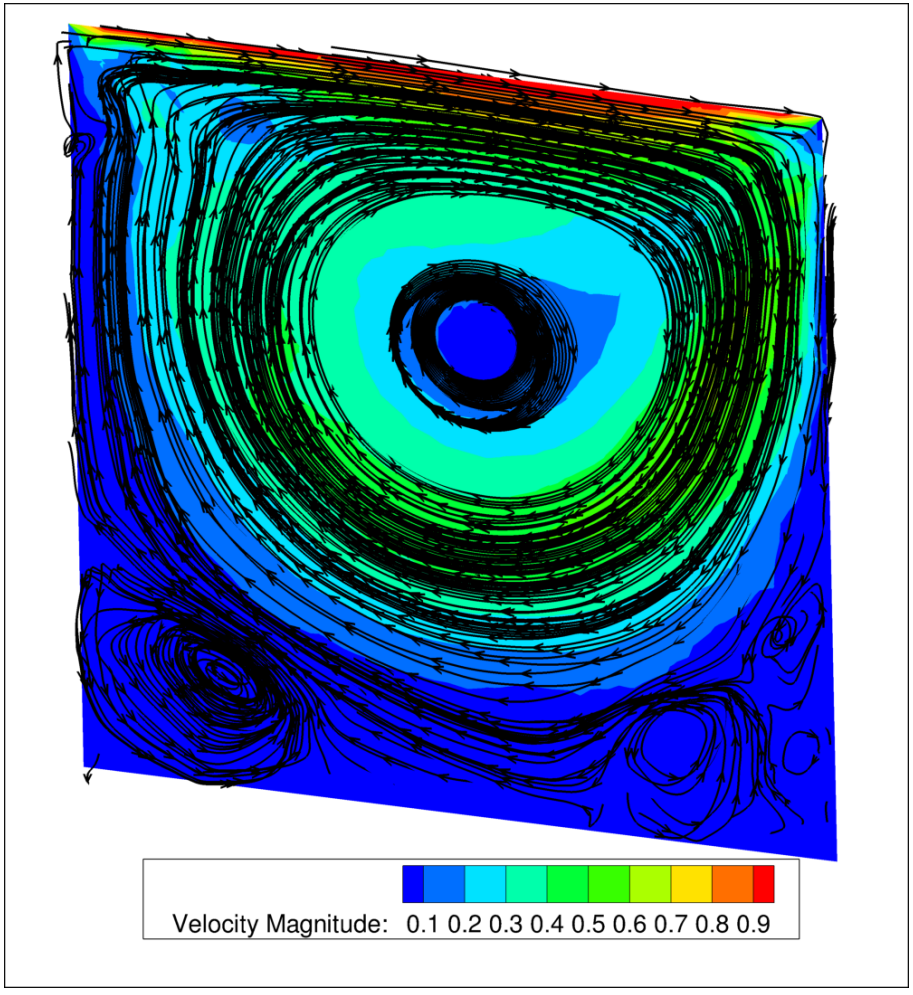

Figure: 3rd order, 354 cells.

3D driven cavity

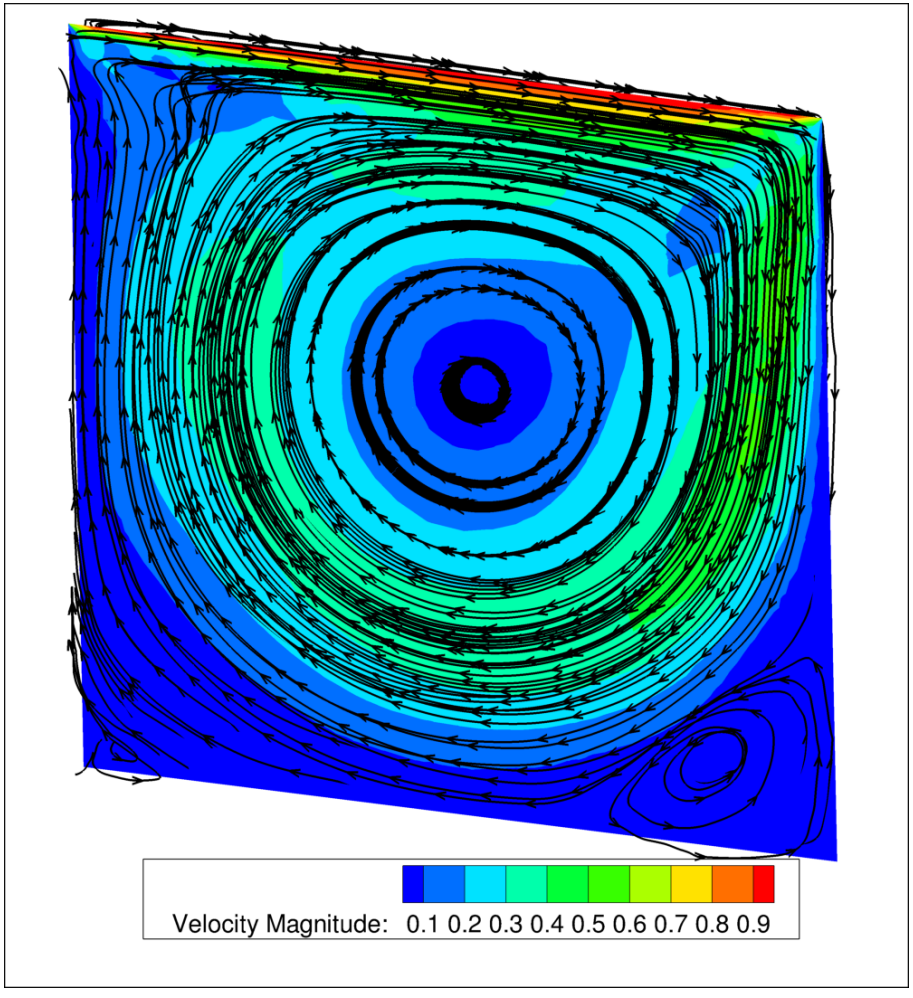

Figure: 4th order, 354 cells.

3D driven cavity

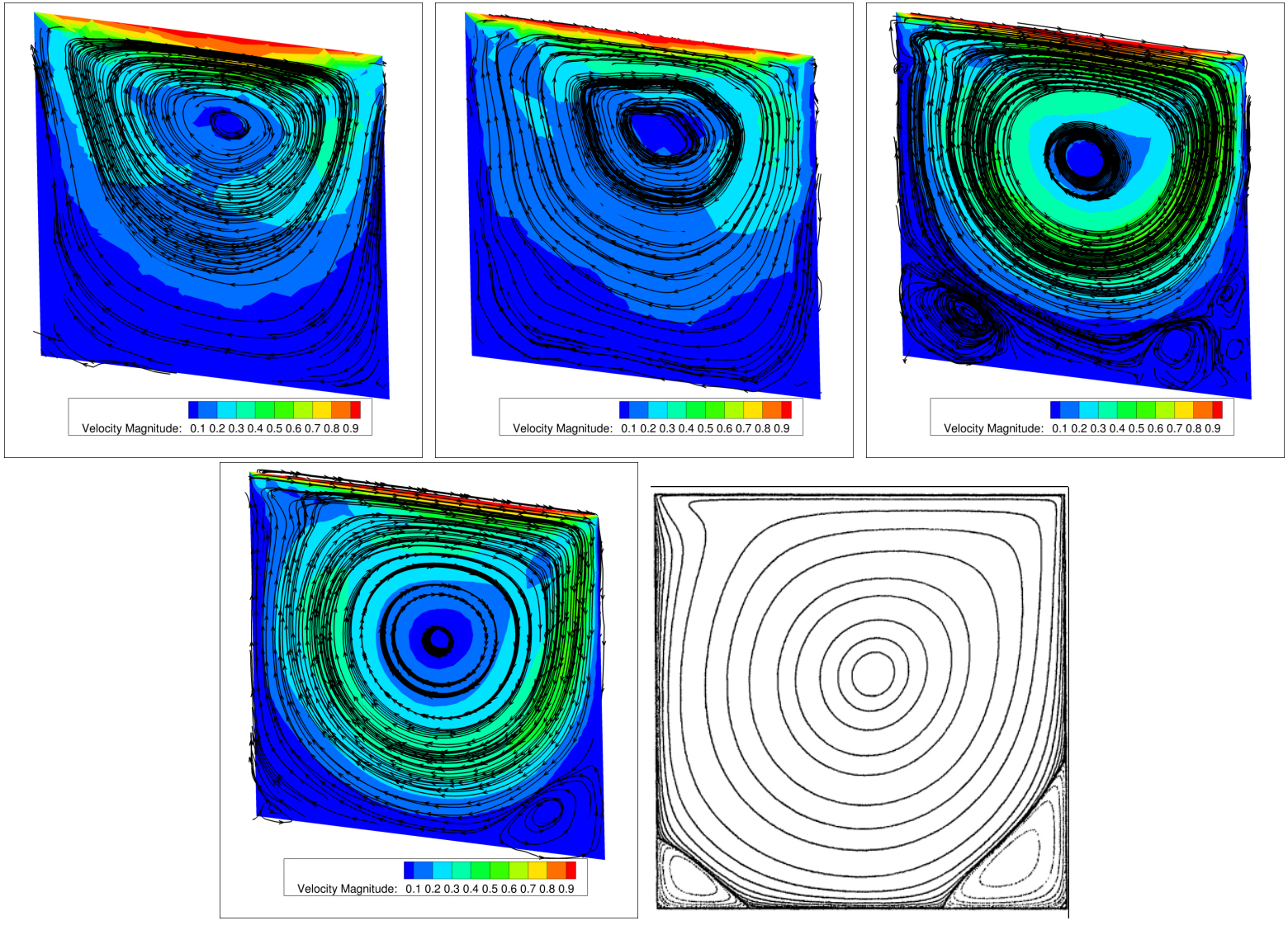

Figure: 3D DG solution with 354 cells c.f. Bruneau & Saad (2006), 1024×1024 grid.

3D driven cavity

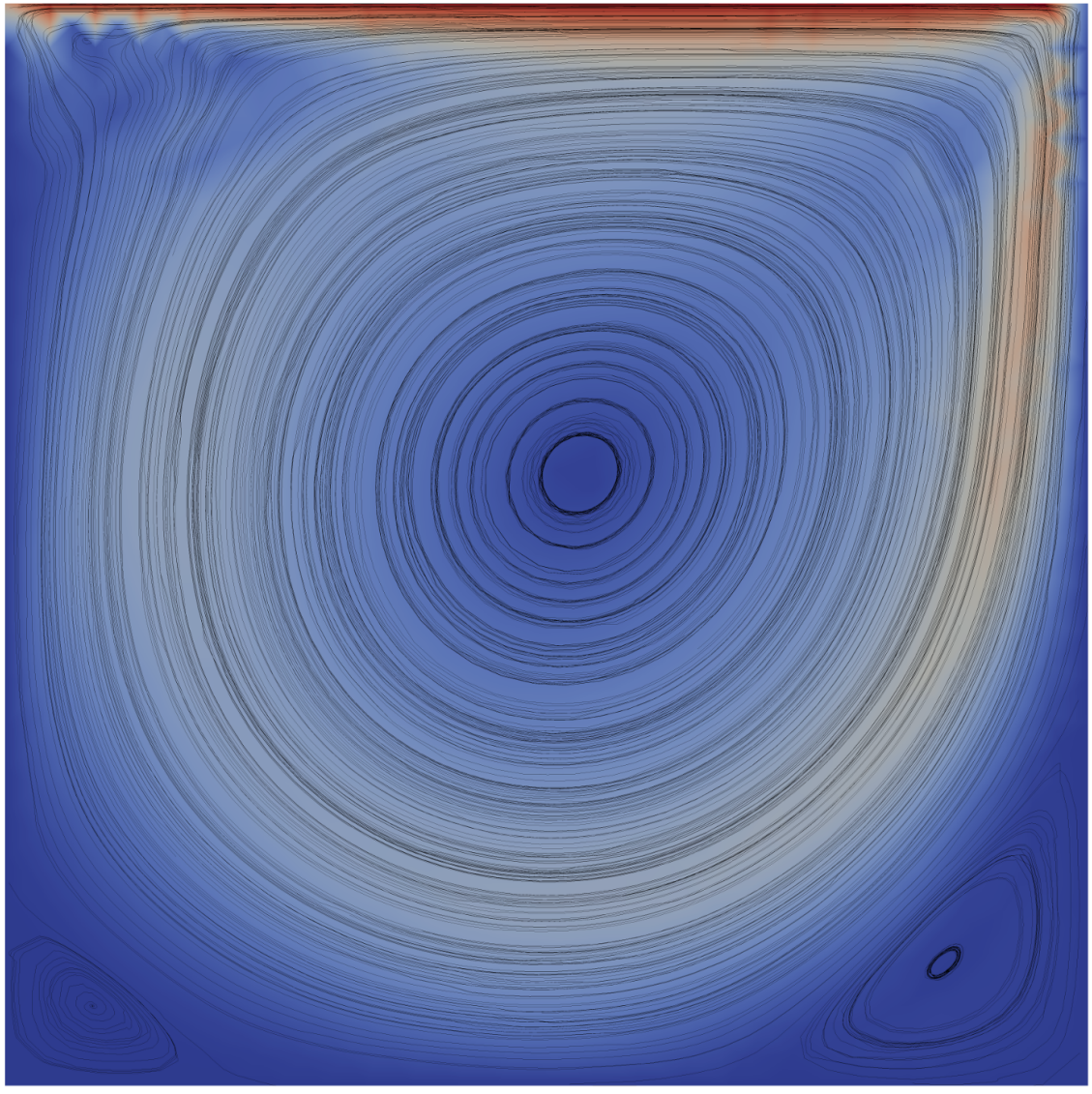

3D B707 cargo hold

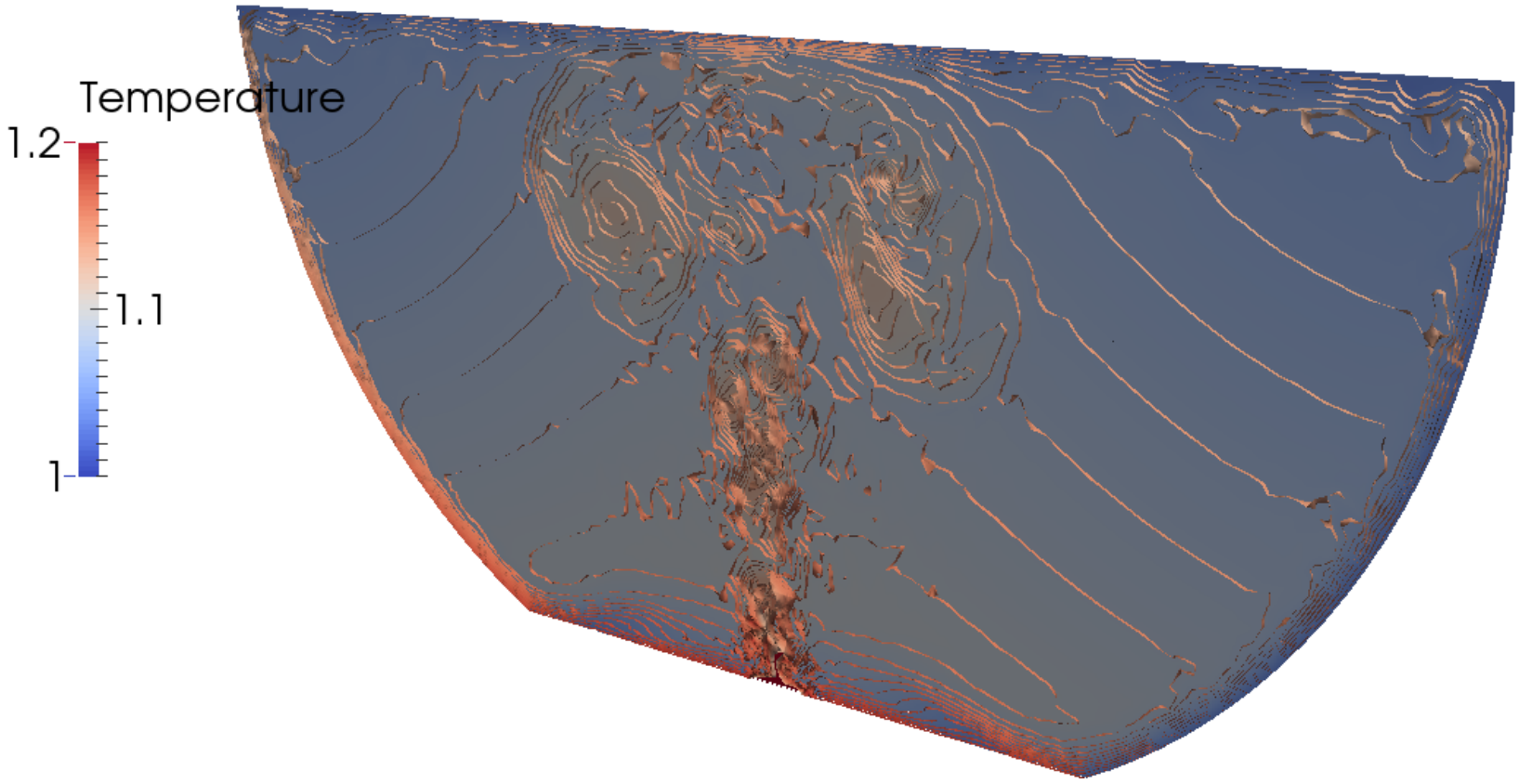

3D B707 cargo hold

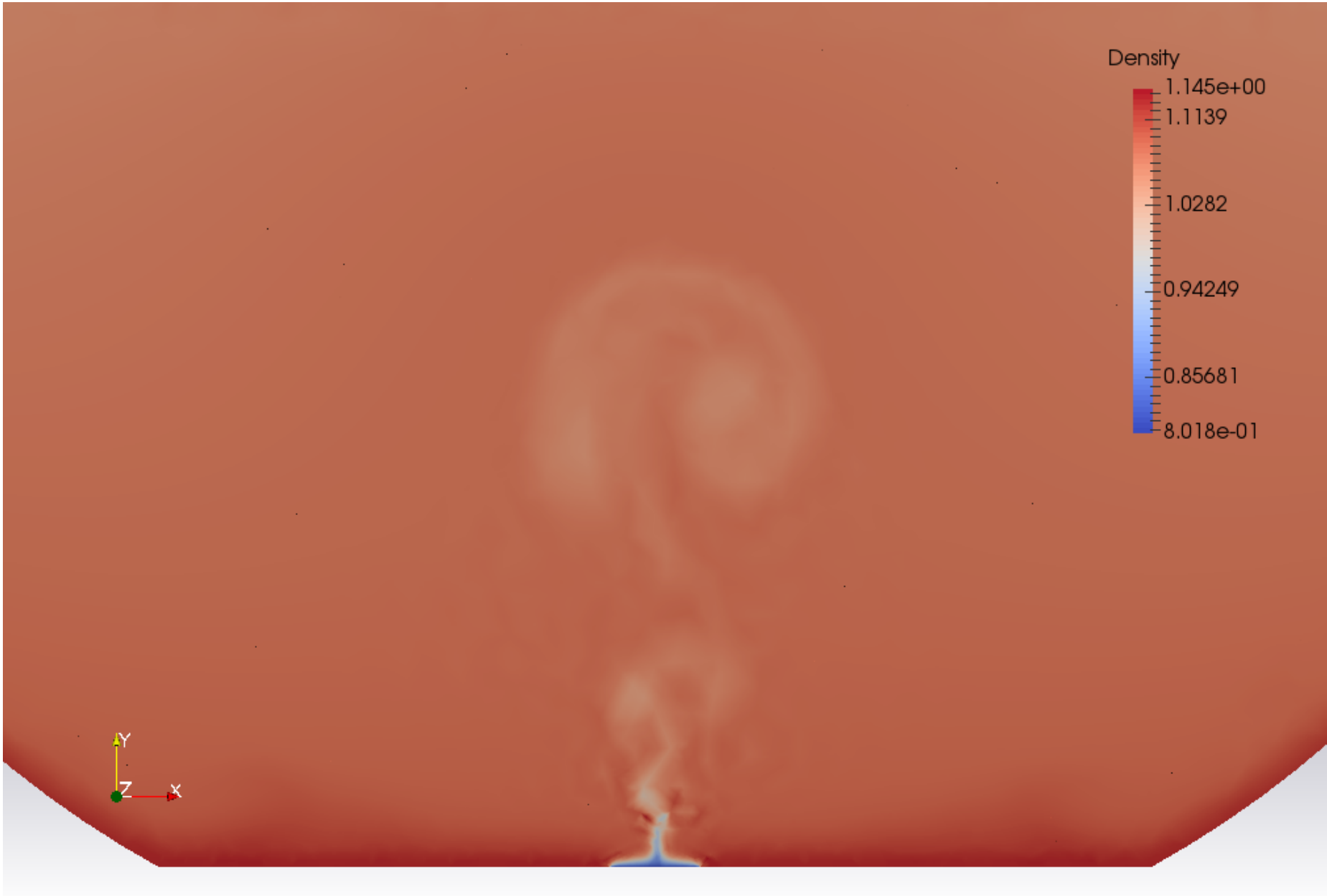

3D B707 cargo hold

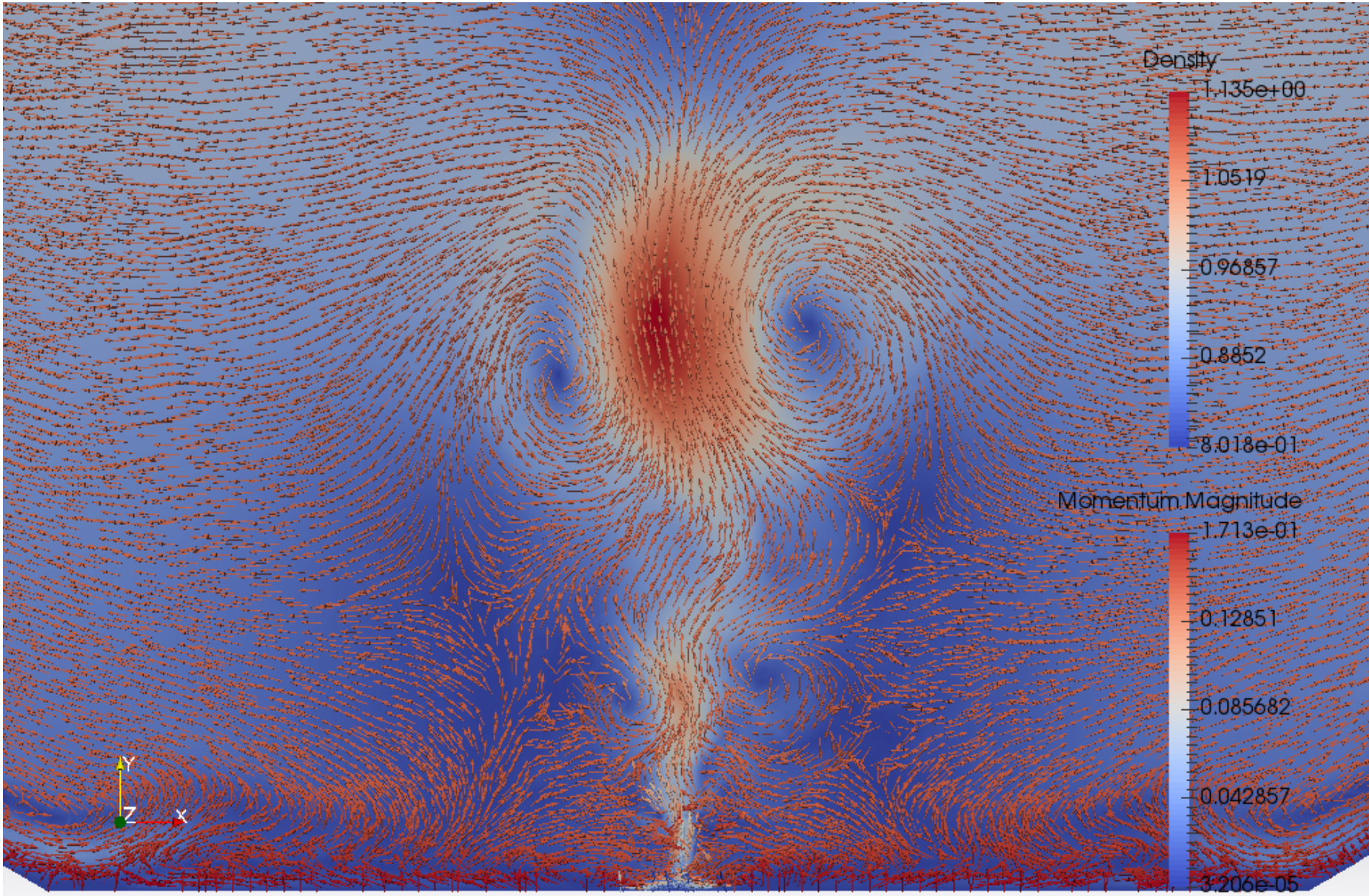

3D B707 cargo hold

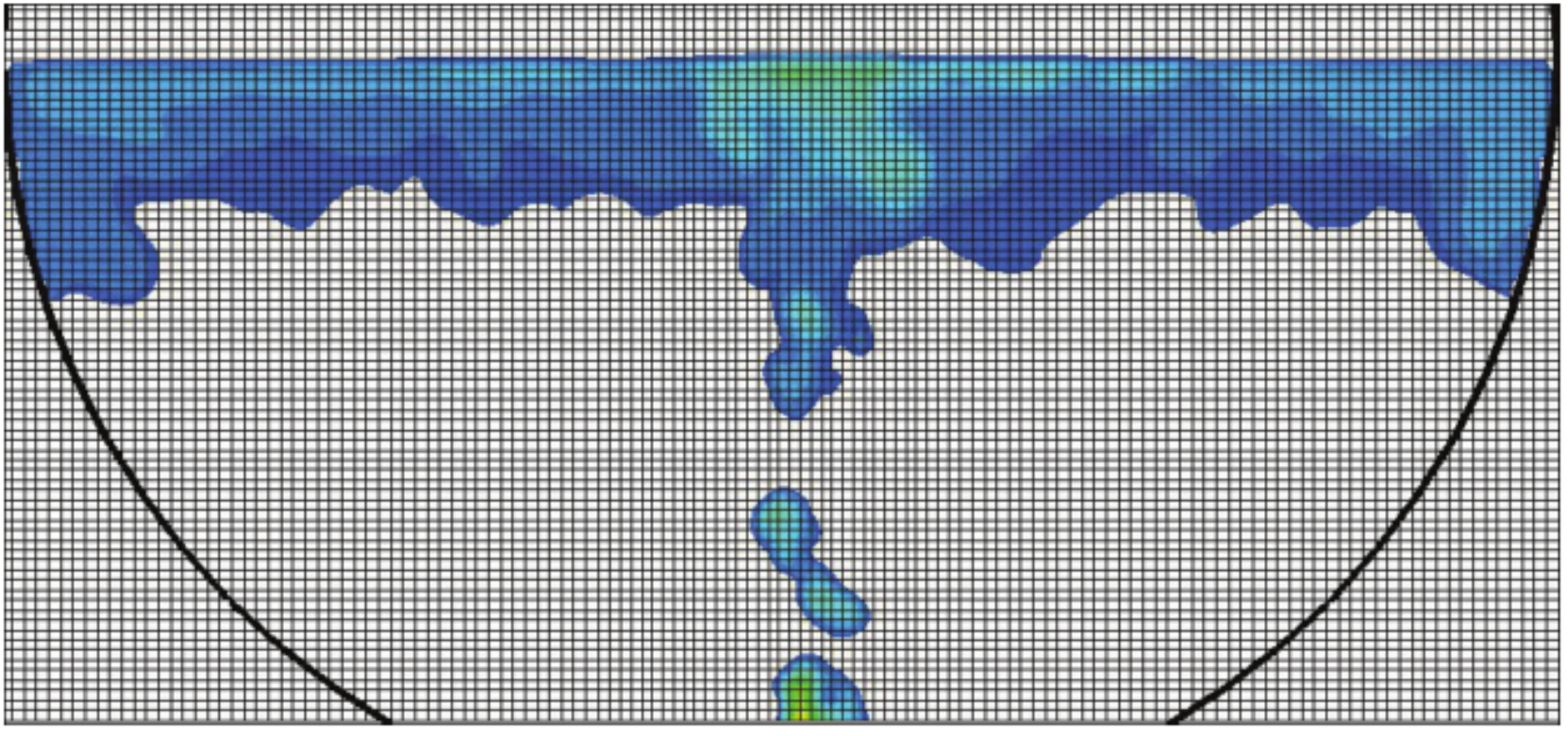

Figure: FDS, *Oztekin*

Software design aspects of a Discontinuous Galerkin solver

Aspects of the Discontinuous Galerkin solver:

- Core flow solver (*it works*):
  - 3D spatial discretization with unstructured meshes and arbitrary order of accuracy, cubature and quadrature rules for evaluating DG terms in the RHS, time integration, ...
- Bells and whistles (*it's useful for complex problems*):
  - Interface to PETSc libraries to handle distributed memory parallelism, nonlinear and linear algebra, Jacobian-Free Newton-Krylov methods.
  - Error-adaptive implicit time stepping.
  - User implemented boundary conditions and volumetric sources to model fires with easy hooks via boost::dll.
  - Separation of discretization details from flow equations: very simple to switch between 1D, 2D, and 3D.
  - Implementation of traditional 2nd order finite volume method.
  - Wide variety of LES and RANS models.

Design

Major software components for DG solver:

- Evaluation of right-hand-side spatial discretization for Discontinuous Galerkin method.
- Time integration
- Nonlinear algebra solver
- Linear algebra solver
- Parallel communication
- File i/o
- User input options
- User-defined boundary/volume functions
- Logging of residuals, debugging info.

Lots of moving parts.

Design patterns - mediator

- Making everything work together without becoming a tightly coupled mess is hard.

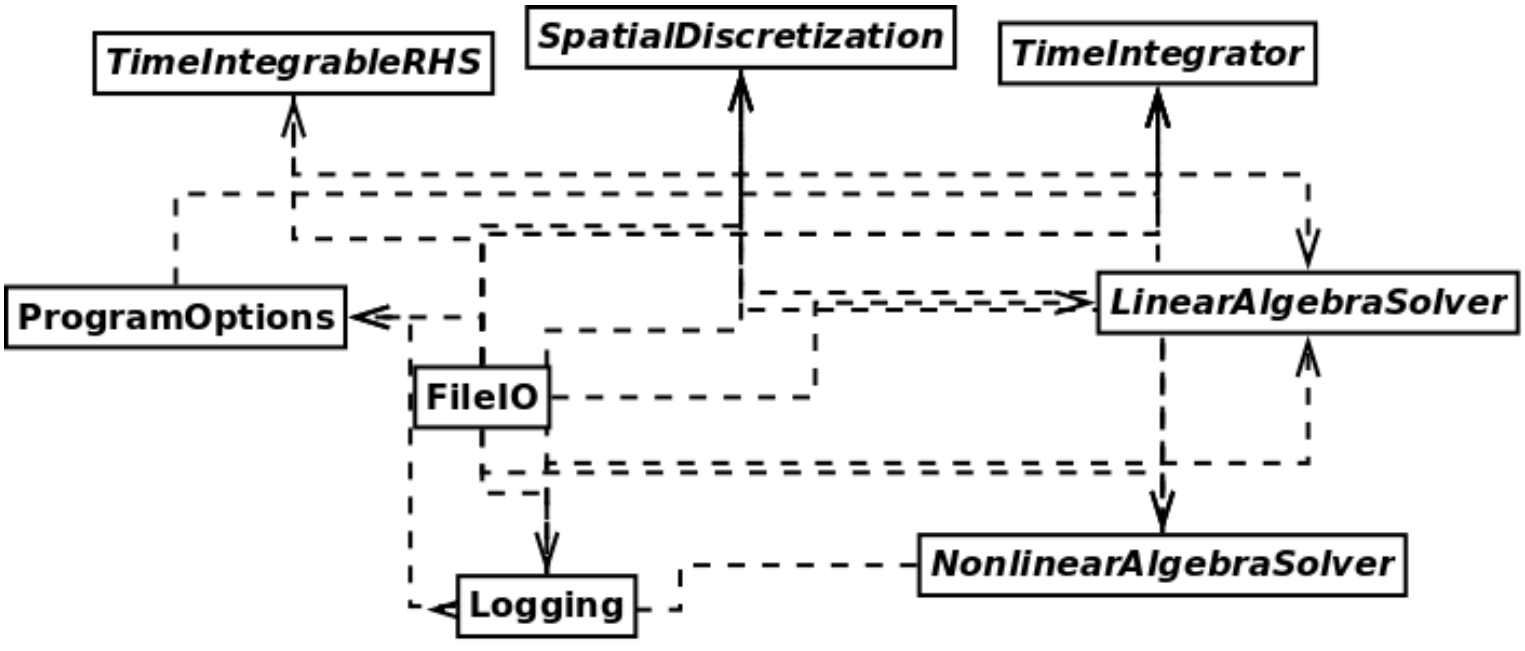

Spaghetti.

- $O(N)$ mutually interacting components require $O(N^2)$ communication complexity.

Design patterns - mediator

- The mediator [1] design pattern encapsulates interactions between classes, which reduces coupling by requiring all communication go through one class.
- Much easier to extend functionality and refactor existing code.
  - *Many-to-many* relationship becomes *one-to-many*.

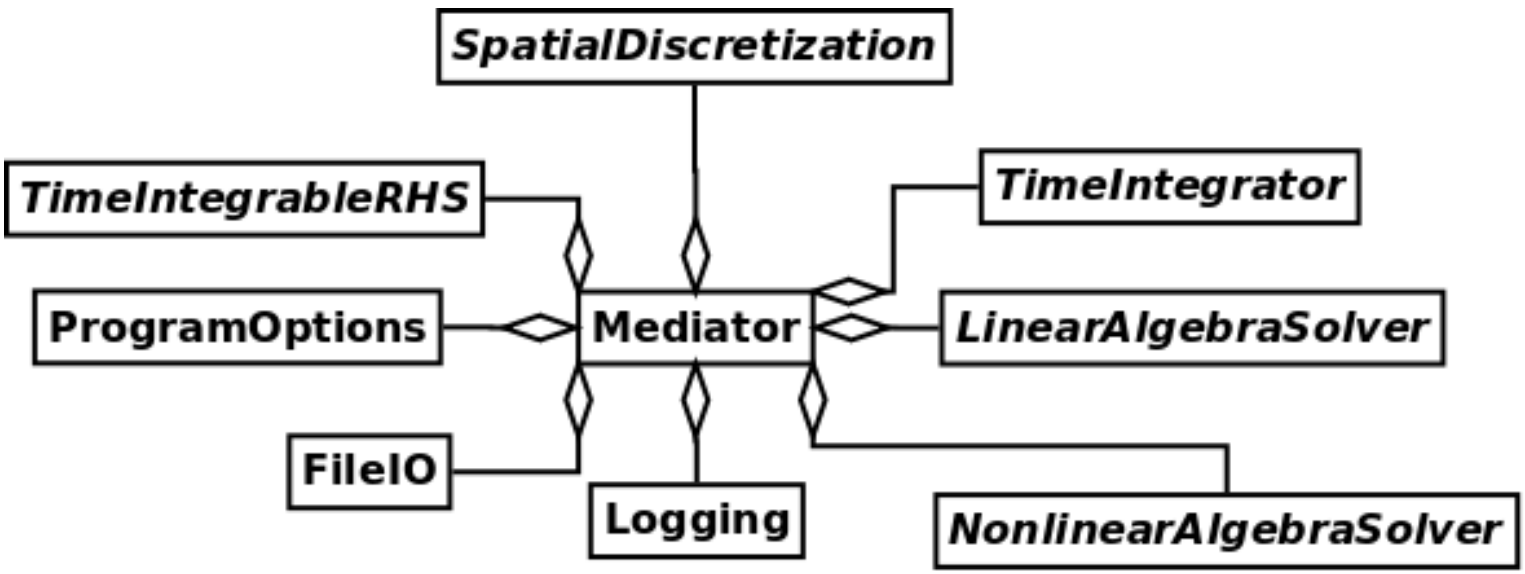

Un-spaghetti'd mediator design pattern.

- I prefer the term puppeteer from Rouson et al.[2]

[1] Design Patterns: Elements of Reusable Object-Oriented Software, 1994

[2] Scientific Software Design: The Object-Oriented Way, 2011

Design - time stepping and algebraic solution hierarchy

- Inheritance or composition where they make sense.
- Time integrators/solvers totally decoupled from spatial residual evaluations:

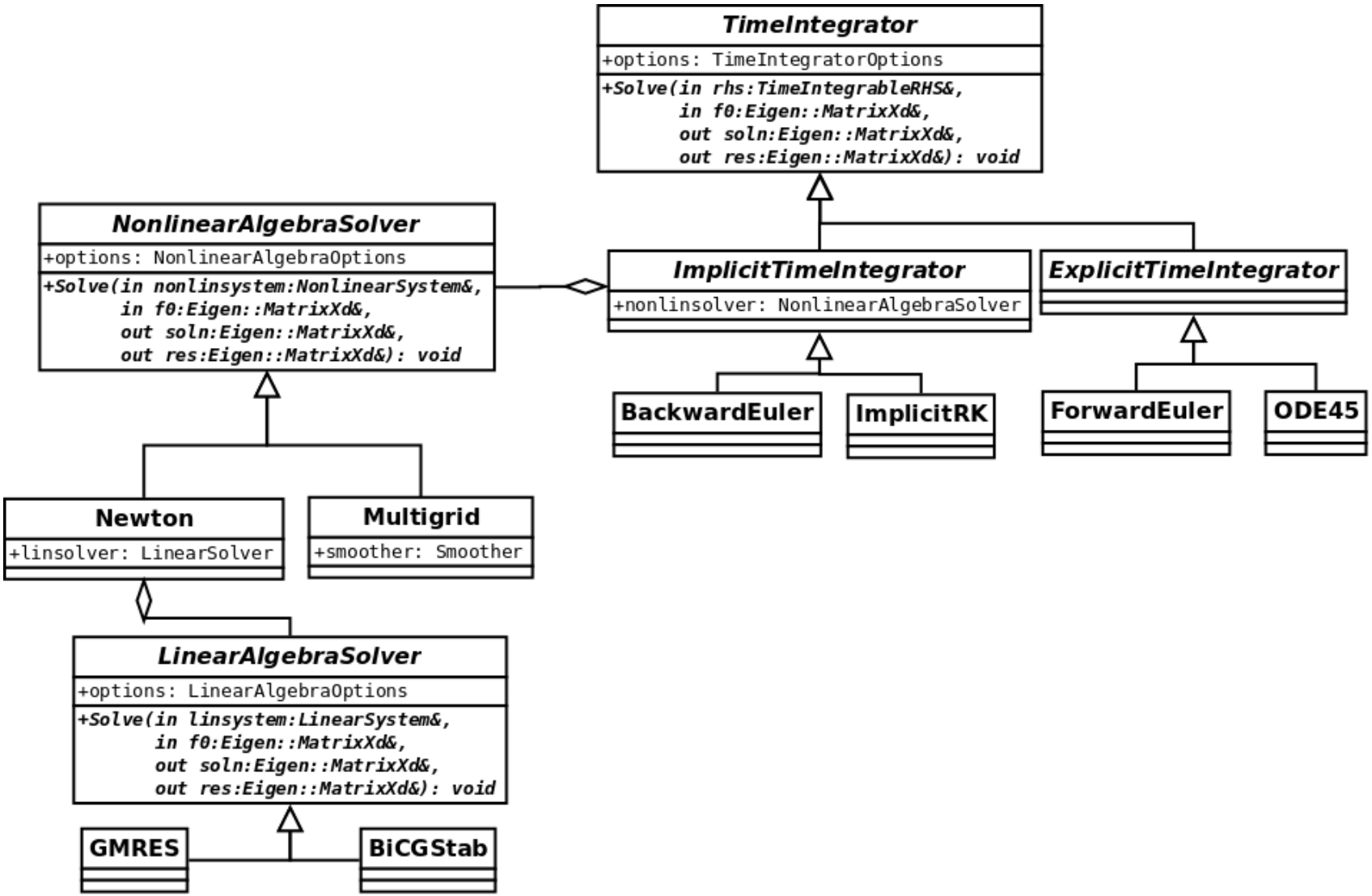

Design - right hand side evaluation

- Inheritance or composition where they make sense.
- Time integrators/solvers totally decoupled from spatial residual evaluations: